Mapping release and propagation areas of permafrost-related rock slope failures in the French Alps: A new methodological approach at regional scale

Maëva Cathala, Florence Magnin, Ludovic Ravanel, Luuk Dorren, Nicolas Zuanon, Frédéric Berger, Franck Bourrier, Philip Deline

Mapping release and propagation areas of permafrost-related rock slope failures in the French Alps: A new methodological approach at regional scale

Cathala M.[1,2], Magnin F.[1], Ravanel L.[1], Dorren L.[3], Zuanon N.[4], Berger F.[5], Bourrier F.[5], Deline P.[1]

[1]EDYTEM, Univ. Savoie Mont-Blanc, CNRS (UMR 5204), 73370 Le Bourget du Lac, France
[2]Alpes Ingé, Saint Vincent de Mercuze, France
[3]Bern University of Applied Sciences BFH-HAFL, Switzerland
[4]A2 Photonic Sensors, Grenoble INP-Minatec, France
[5]INRAE, Grenoble, France

Correspondence to: Maëva Cathala (maeva.cathala@univ-smb.fr)
5 Boulevard de la Mer Caspienne 73370 Le Bourget du Lac (France)
ORCID: 0000-0001-7212-3104

Abstract

Rock slope failure (RSF) from permafrost-affected rockwall is an emerging threat for human lives and infrastructure which raises a need for RSF hazards assessment in the alpine environment. This study proposes the first mapping approach of RSF release and propagation areas in the French Alps.

By analysing a unique RSF database (1389 recent events in the Mont Blanc massif), we determine 3 levels of RSF Susceptibility Indexes (RSI) to map the potential release areas. We highlight a strong link between RSF and permafrost: 99% of RSFs occurred from rockwalls with Mean Annual Rock Surface Temperature (MARST) ≤ 3°C and 35% with MARST from -2 to 0°C.

The release area maps (34 km² to 284 km² depending on the RSI) are used as input in a simple propagation model (*RockavELA*), using a dimensionless area-based energy line principle to map propagation areas (*i.e.* reach susceptibility) of potential RSFs. Three propagation limits are proposed, fitting the propagation characteristics of another RSF database containing 3497 events observed throughout the European Alps with heterogeneous propagation substrates, and merged with 48 additional events from the French Alps high mountains. *RockavELA* reproduced runout extent of 20 high mountain RSFs with < 50% of frontal and lateral error. Output maps show little sensitivity to the propagation limits (< 25% difference between the high and low propagation limits).

This work is a preliminary step to identify potential hazardous hot spots in the French Alps, and proposes a novel approach that could be implemented in other mountain ranges.

Keywords: rock slope failure, permafrost hazard, GIS, regional mapping, runout modelling

Statements and Declarations

Competing interest: The authors declare no competing interests.

Acknowledgments

This study was funded by the Alpes Ingé SARL (http://alpes-inge.com/) and the French Agency for Research and Technology (ANRT) under the PhD CIFRE (*Convention Industrielle de Formation par la REcherche*) scholarship n°2019/1803. The authors further acknowledge Marco Marcer for upscaling the SAFRAN air temperature data used for the Mean Annual Rock Surface Temperature mapping model. The *RockTheAlps database* is funded by the European Regional Development Fund, Alpine Space Program, Project "ROCKtheALPS".

Authors contributions

All authors contributed to the study conception and design. Maëva CATHALA conducted data analysis, took part in the development and calibration of *RockavELA* model, and provided results interpretations. She wrote the first draft of the manuscript and designed all the figures. Florence MAGNIN modelled and designed the Mean Annual Rock Surface Temperatures maps, participated to the databases analysis and to the results interpretation and synthesis. Luuk DORREN developed the principles of propagation modelling in *RockavELA* and he developed the numerical code with Nicolas ZUANON. Frédéric BERGER conducted the analysis of *RockTheAlps database* and also contributed to the development of *RockavELA*. Franck BOURRIER contributed in the interpretation of the results. Ludovic RAVANEL carried out the data collection for *Mont-Blanc massif Rock Slope Failure database* used in this study. Philip DELINE contributed in the interpretation of the results. All authors commented on previous versions of the manuscript, read and approved the final manuscript.

1 Introduction

High mountain environments are increasingly impacted by the effects of climate change (IPCC 2019). The temperature has already risen by 2°C in the European Alps between the end of the 19th and the beginning of the 21st century with an acceleration of the warming since the 1980s (Auer et al. 2007; Einhorn et al. 2015). The main impacts of the rising air temperature on the Alpine cryosphere are glacial retreat (Zemp et al. 2006), permafrost degradation (Biskaborn et al. 2019; Haberkorn et al. 2021), thinning and shorter duration of the snowpack (*e.g.*, Verfaillie et al. 2018), and elevation of the rain-snow limit (*e.g.*, Böhm et al. 2010).

The loss of glacier area and volume since the end of the Little Ice Age (LIA) is significant and has been clearly accelerating since the 1980s (Zemp et al. 2006; Huss 2012; Zekollari et al. 2019). Permafrost degradation is also an important marker of cryosphere changes in recent decades and the temperature time series in boreholes have shown a global degradation of permafrost, notably in ice-poor ground such as rockwalls and bedrock (Etzelmüller et al. 2020; Haberkorn et al. 2021).

These ongoing processes lead to Rock Slopes Failures (RSFs; Fischer et al. 2006; Gruber and Haeberli 2007; Huggel et al. 2010; Hartmeyer et al. 2020; Deline et al. 2021), defined in this study as detachment of a rock mass, whatever its volume. Investigations in the Europeans Alps have shown an increase in RSFs occurring as rockfalls, often defined as rock mass detachment > 100 m^3 (Ravanel and Deline 2011; Fischer et al. 2012; Temme 2015; Paranunzio et al. 2019), especially during summer heatwaves (Ravanel et al. 2010, 2017; Legay et al. 2021). Larger events can reach several millions of m^3, sometimes mixed with ice, and are often defined as rock avalanches or rock/ice avalanches (Evans et al. 1989; Huggel et al. 2005; Jibson et al. 2006; Shugar et al. 2021). These major events sometimes generate cascading processes (Haeberli et al. 2016a) resulting in massive destruction down valley and many casualties (*e.g.*, Byers et al. 2018; Walter et al. 2020; Zheng et al. 2021).

Beyond the geological (lithology, fractures) and topographical conditions (slope, aspect, altitude) playing a role in the occurrence of RSF (Ballantyne 2002), permafrost degradation – which occurs through thickening of the active layer (*i.e.* the subsurface layer freezing and thawing throughout the year) and permafrost warming toward 0°C (Gruber and Haeberli 2007) - is thought to play a key-role through the mechanical alteration of the intact rock mass and ice-filled fractures (Krautblatter et al. 2013; Mamot et al. 2018, 2021). Many observed events have thus been already attributed to permafrost degradation (Deline et al. 2013; Ravanel et al. 2013; Knoflach et al. 2021; Etzelmüller et al. 2022). Some studies also point out the possible role of water infiltration and water flow that could locally accelerate cleft ice erosion and favour high hydrostatic pressure at ice-sealed fractures (Fischer et al. 2010; Hasler et al. 2011a; Magnin and Josnin 2021).

RSF could be a threat for human lives and infrastructure (Haeberli et al. 2016b) that are located on unstable permafrost-affected slopes (Ravanel et al. 2013; Duvillard et al. 2015, 2019) or in their propagation zone. Identifying spatial susceptibility of RSF occurrence and propagation is thus becoming a key challenge in hazard and risk assessment.

Previous research proposes regional release and runout zonation for different gravitational hazards such as landslides (*e.g.* Mergili et al. 2019), debris flows (*e.g.*, Mergili et al. 2017), rockfalls (*e.g.*, Michoud et al. 2012), rock avalanches (*e.g.*

Scheidegger 1973), large rock/ice avalanches (*e.g.* Noetzli et al. 2006), Glacial Lakes Outburst Floods (GLOF; *e.g.* Huggel et al. 2003; Furian et al. 2021) and multi hazards assessment (*e.g.* Gruber and Mergili 2013). Some approaches consider only the source area (*e.g.* Loye et al. 2009), whereas others consider also the runout areas (*e.g.* Horton et al. 2013; Mergili et al. 2019). These regional approaches require minimal input data and parameters to estimate deposit areas (*e.g.* Noetzli et al. 2006; Horton et al. 2013), notably topographical factors and the length of the propagation area (Heim 1932; Lied 1977; Hsü 1975; Evans and Hungr 1993). In contrast, physics-based models require more input such as volume, friction parameters, initial condition, rock density, but allow in depth analysis at a local scale (Mergili et al. 2014).

The identification of release and propagation areas is a first step in risk assessment. It can lead to the development of early warning systems to further prevent risks (Budimir et al. 2019; Pecoraro et al. 2019; Guzzetti et al. 2020). However, in the context of climate change and evolving cryosphere, new areas may become at risk. It is therefore necessary to assess permafrost distribution, build up an RSF inventory and analyse the conditions under which they occur. For this purpose, the Glacier and Permafrost Hazards in Mountain (GAPHAZ) group proposes guidelines for hazard assessment, which are (i) to assess rockwall stability and triggering conditions of RSFs, and (ii) to map potential hazards in mountain regions (GAPHAZ 2017; Allen et al. 2022). Such integrated approaches for permafrost hazard assessment require basic knowledge of permafrost and mass movement distribution, but quantitative characterisation of the RSF release conditions and propagation are often missing.

Our study intends following the GAPHAZ principles to make a first step towards assessment of hazardous permafrost-affected rockwalls in the French Alps. The aims of this study are thus to map (i) the release areas of potential RSFs in the current context of permafrost degradation, and (ii) their possible propagation areas for the entire French Alps.

To do so, we use a large inventory (1389 events) of RSFs (volumes 100-80,000 m^3) documented in the Mont-Blanc massif between 2007 and 2019 and a predicted rockwall permafrost map. A statistical analysis of this database allows us to determine areas most prone to failure according to their topographical and permafrost conditions and to determine 3 levels of *Rock slope failure Susceptibility Indexes* (RSI). In the next step, RSI maps are used as input for a simple propagation model (*RockavELA*) developed in order to map the propagation areas of potential events. The model uses a dimensionless area-based energy line principle and is calibrated with an RSF database (3497 events; volumes of the largest single projectiles ranging from 100m^3 to 292,000 m^3) from the whole Alpine range (*Interreg Alpine Space* project "RockTheAlps" 2016-2019) and 48 other events (volumes ranging from 0.02m^3 to 1000 m^3) inventoried in the French Alps at high elevation (> 2000 m a.s.l.).

This work provides a first overview of RSF susceptibility from permafrost-affected rockwalls, as well as areas potentially impacted. We propose a first application of this method in the French Alps high mountains. It is a first step to support a risk assessment strategy in the climate change context and could ultimately serve as a tool for decision-makers and stakeholders to assess potential hot spots.

2 Study area: The French Alps

The French Alps constitute the western part of the European Alps (Fig. 1). They extend from the Mont-Blanc Massif (MBM) to the Mediterranean coast, and host 25 peaks above 4000 m a.s.l. The three highest massifs are Mont-Blanc, Écrins and Vanoise, culminating at the Mont Blanc (4808 m a.s.l.), Barre des Écrins (4102 m a.s.l.) and Grande Casse (3855 m a.s.l.), respectively. The climatic context of the French Alps is roughly divided by the 45th North parallel: the north-western part is wetter because of the depressions coming from the Atlantic Ocean, while the Southern Alps are dryer due to the Mediterranean influence (Bénévent 1926; Gottardi 2009).

581 glaciers covering a surface area of 275.4 km² were present in the French Alps during the period 2006-2009, the largest one being the Mer de Glace (30.5 km²) in the MBM (Gardent et al. 2014). The mean front altitude of these glaciers is 2840 m a.s.l., with the glacier des Bossons being the lowest (*c*. 1650 m in 2022) in the MBM. Glaciers lost 50% of their surface area between 1850 and 2006-2009, of which *c*. 25% was between 1967-1971 and 2006-2009. Glacial retreat has been accelerating for several decades and will continue to do so in the coming decades (Zekollari et al. 2019), leading to the formation of lakes in recently deglaciated areas (Magnin et al. 2020; Cathala et al. 2021).

The lower altitudinal limit of cold continuous rockwall permafrost is *c*. 2800 ± 200 m and 3300 ± 300 m a.s.l. on the north and south faces, respectively, and *c*. 2500 ± 200 m and 3000 ± 300 m for warm discontinuous permafrost (Magnin et al. 2015a). In surficial deposits, this limit is in the 2300 – 2500 m range, depending on aspect and regional precipitation (Marcer et al. 2017). Mapping of rockwall permafrost has been carried out only for the MBM, by generalizing the "Rock model" from Boeckli et al. (2012) with a 4-m resolution DEM. In this study, the rockwall predicted permafrost map has been extended to the whole French Alps with the same approach (see Sect. 3.2).

The lower limit of permafrost tends to rise, and modelling suggests that it could disappear from south faces at least up to 4300 m a.s.l. while warm permafrost could extend at least up to 3850 m a.s.l in the north faces (Magnin et al. 2017). The number of RSFs may therefore further increase in high mountain environments over the coming decades. Studies from the MBM have indeed already shown this increase in conjunction with atmospheric warming and permafrost degradation (Ravanel and Deline 2011; Ravanel et al. 2017).

The French Alps have not yet been investigated at a regional scale to identify areas at risk due to RSFs under current and future climate warming conditions. However, the MBM is very well investigated and constitutes a study area that provides an opportunity to improve knowledge about the RSF triggering conditions (Ravanel et al. 2011, 2017; Legay et al. 2021).

In this study, we divide the French Alps in 4 zones to allow a more detailed analysis of each area according to their characteristics (such as lithology, latitude, climate, glacier and permafrost extent; Fig.1). As our study focuses on periglacial processes, we kept in our analysis only the areas above 1500m a.s.l.

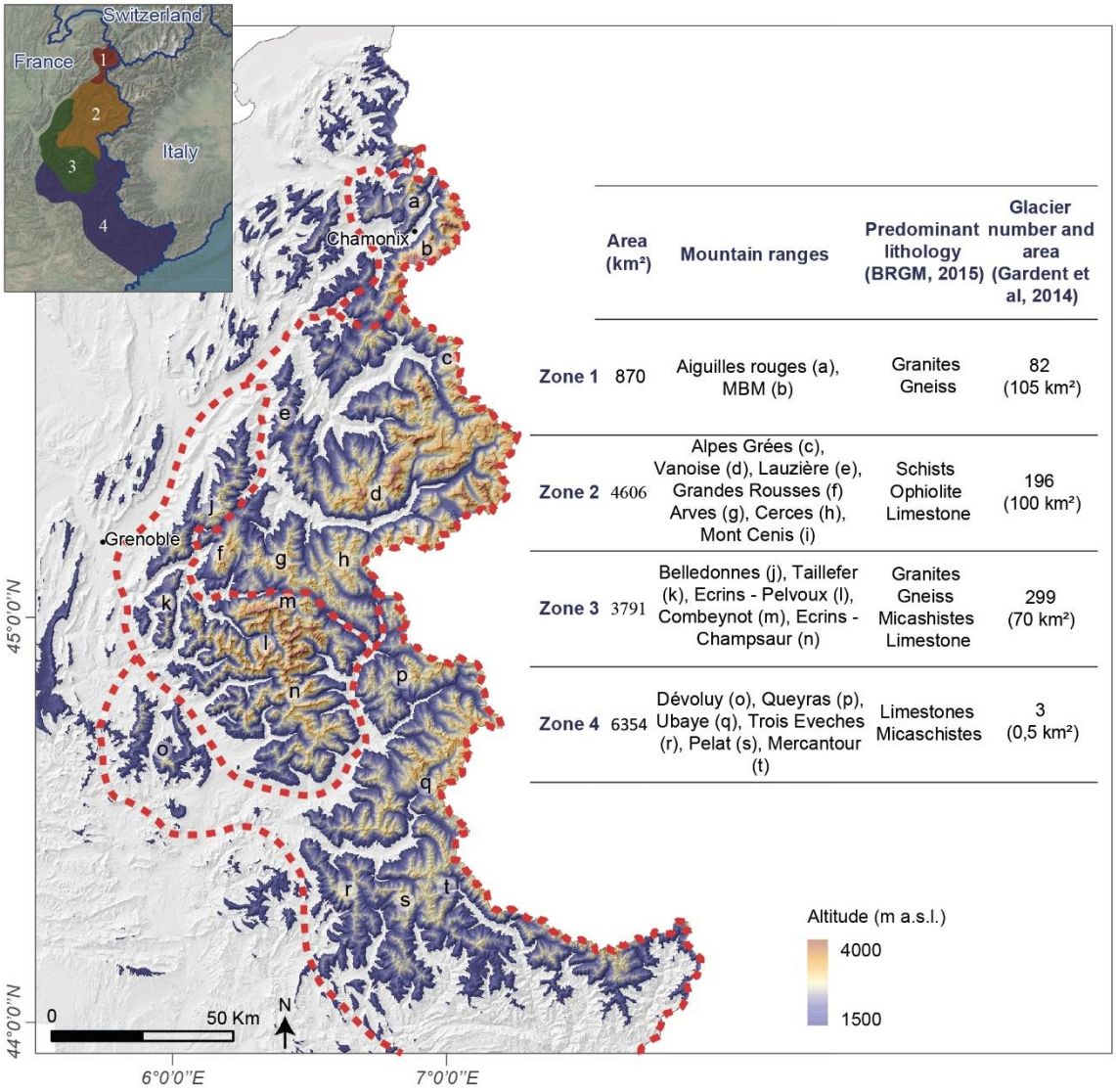

	Area (km²)	Mountain ranges	Predominant lithology (BRGM, 2015)	Glacier number and area (Gardent et al, 2014)
Zone 1	870	Aiguilles rouges (a), MBM (b)	Granites Gneiss	82 (105 km²)
Zone 2	4606	Alpes Grées (c), Vanoise (d), Lauzière (e), Grandes Rousses (f) Arves (g), Cerces (h), Mont Cenis (i)	Schists Ophiolite Limestone	196 (100 km²)
Zone 3	3791	Belledonnes (j), Taillefer (k), Ecrins - Pelvoux (l), Combeynot (m), Ecrins - Champsaur (n)	Granites Gneiss Micashistes Limestone	299 (70 km²)
Zone 4	6354	Dévoluy (o), Queyras (p), Ubaye (q), Trois Eveches (r), Pelat (s), Mercantour (t)	Limestones Micaschistes	3 (0,5 km²)

Fig.1 The French Alps and the 4 divisions used in this study. The area (> 1500m a.s.l), names of mountain ranges, lithology and number of glaciers are given for each division (With a 25m resolution DEM from *Institut National de l'information Géographique et Forestière (IGN)*)

3 Methods and data

Our approach comprises 3 steps. First, we analyse the RSF triggering conditions using the *MBM RSF database* (1389 events) for which we retrieve slope conditions from a 25-m DEM at each event location and permafrost conditions retrieved from a predicted Mean Annual Rock Surface Temperature (MARST) map (Sect. 3.1). Secondly, we map potential release areas according to the conditions the most likely to trigger RSFs (Sect. 3.2.1). In a third step, we analyse RSF propagation characteristics using 48 events that have recently occurred in high mountain areas (*High Mountain database*) and 3497 at lower

altitudes (*RockTheAlps database;* Sect. 3.2.2). Since the *High Mountain database* and the *RockTheAlps database* display similar propagation characteristics, they are merged in the *Propagation database* to fit propagation limits in a simple model (*RockavELA*). The calibration and evaluation of the frontal and lateral extent of the modelled deposition area are carried out using 20 events from the *High Mountain database*. These different steps are detailed in Fig.2.

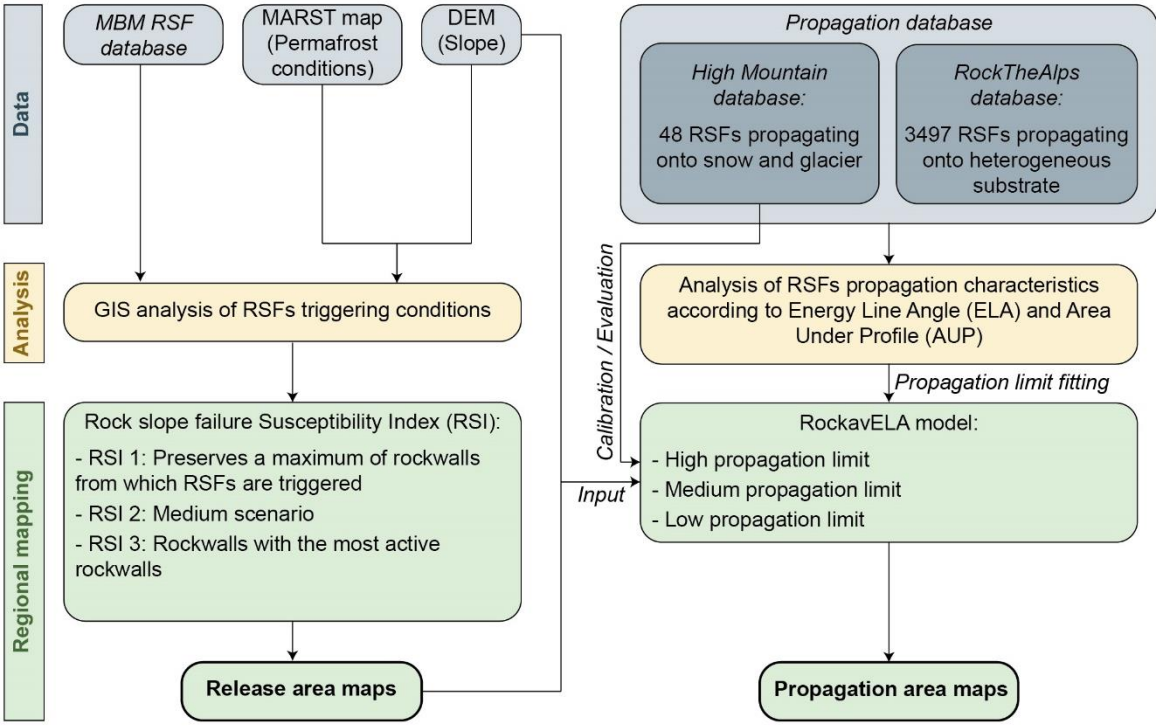

Fig.2 Presentation of the approach proposed in our study, with the data and method used for regional mapping of release and propagation areas

3.1 Data

3.1.1 DEM and predicted permafrost distribution map

In this study, we use a 25-m resolution DEM provided by IGN (*Institut national de l'information Géographique et Forestière*), whose data were acquired mainly by radar technology between 2009 and 2011. While DEMs at higher resolution exist for some areas, it is the only homogeneous DEM covering the entire French Alps so we chose it to ensure consistency between all steps of this work.

The permafrost distribution is modelled with the multiple linear regression "Rock model" calibrated by Boeckli et al. (2012) with 53 MARST measurement points spread across the European Alps. This model explains the MARST with Potential Incoming Solar Radiation (PISR) values and Mean Annual Air Temperature (MAAT) values at MARST measurement points. Boeckli et al. (2012) further applied a temperature offset to the MARST to represent possible temperature at depth (Mean Annual Rock Temperature, MART) calculated according to sun-exposure based on Hasler et al. (2011b). The MART is then

converted into an index depicting the favourability of rockwalls to permafrost occurrence using the standard deviation of the rock model. This approach has been implemented in the Mont Blanc massif in only one previous study (Magnin et al. 2015a) and evaluated against distributed Electrical Resistivity Tomography surveys (Magnin et al. 2015b).

In this study, we implement the "Rock model" on the 25-m DEM with the 1981-2010 MAAT to represent current permafrost conditions. The MAAT is provided by *Météo France* using the SAFRAN model (Durand et al. 1993) that represents daily air temperature according to 300-m elevation bands over the French Alps and upscaled to the 25-m DEM. Solar radiation is calculated with ArcGIS (ESRI®) tools following Boeckli et al. (2012) approach. We use the predicted MARST values for slopes > 30° here considered as "steep slopes" considering the rather coarse DEM resolution. Permafrost is typically expected for MARST < 3°C (Hasler et al. 2011b) and we thus expect warm and highly discontinuous permafrost conditions where the predicted MARST suggests temperatures between -2 and 3°C. An example of the final predicted MARST map for the MBM is shown in Fig. 3.

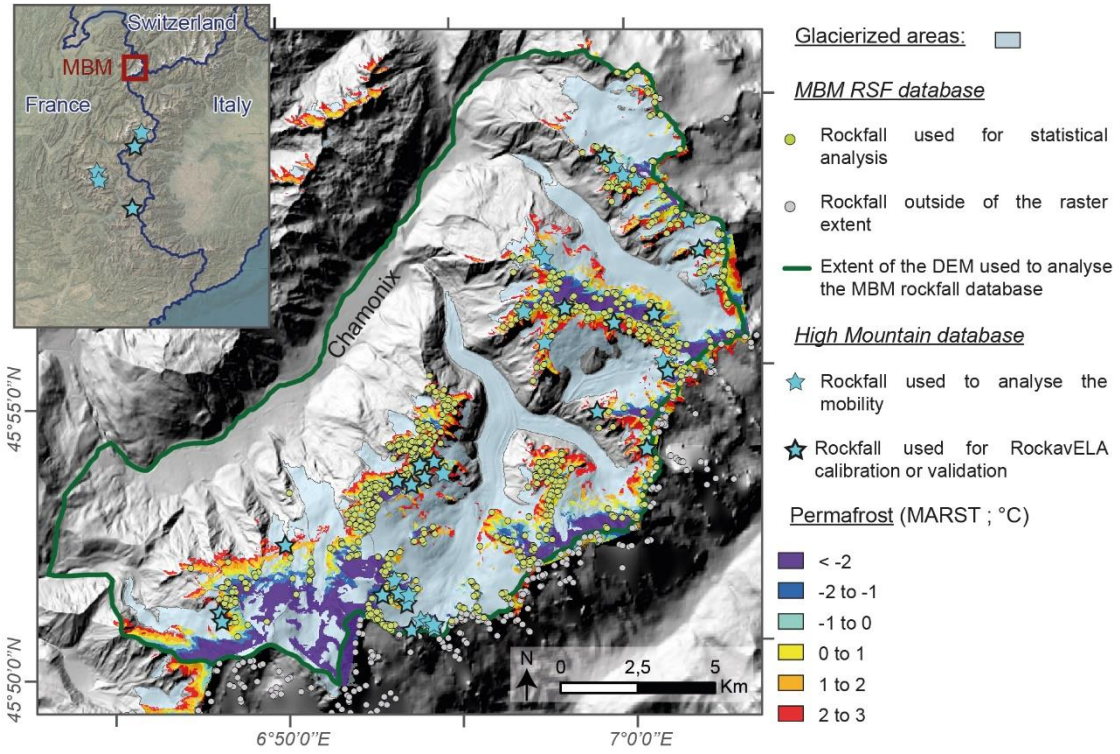

Fig.3 The *Mont-Blanc massif RSF database* and *High Mountain database*, glacierized areas and predicted Mean Annual Rock Surface Temperature (MARST) map used in this study. (With a 25-m resolution DEM from IGN)

3.1.2 RSF databases

MBM RSF database

In this study, we use the *MBM RSF database*, which contains 1389 RSFs recorded in the MBM by a network of observers over a 15-year period (2007-2021; Fig. 3). The network comprises mountain practitioners who report information about RSFs they

have observed *via* mails, apps or oral communication; these observations are then verified and supplemented during fieldwork (Ravanel and Deline 2013). The volumes of these RSFs range from 100 m^3 to 80,000 m^3, with a mean volume of 1218 m^3 and a median value of 400 m^3. For each event, we know the geographical coordinates, which enables them to be projected in a GIS.

Propagation database

First, we use the *High Mountain database* composed by 48 RSFs (> 100 m^3) for which we know the exact location of the scar and the front of the deposit identified with satellite images and verified during fieldwork (Supplementary materials Fig. S1). Most of these events (43) are from the *MBM RSF database* (Fig. 3); the others (5) were recorded in the Vanoise, Écrins and Ubaye massifs between 2017 and 2020. When Sentinel-2 satellite images were available at the date of the RSF and usable (no clouds), we used them to reconstruct the precise geometry of the deposit. This was the case for 20 events of the *High Mountain database*.

Among these 48 events, 45 have travelled onto glaciers, sometimes covered by snow or rock debris; the others have propagated onto bedrock (*e.g.*, Vallon d'Étache; Supplementary materials Fig. S2). The RSF propagation distance is determined using the Energy Line Angle (ELA), of which the calculation is detailed in Section 3.2.2. Among these 48 events, the smallest ELA is 16.8°, implying a relatively high mobility of the RSF (Vallonbrun; Supplementary materials Fig. S3). In contrast, the RSFs with the lowest mobility have an ELA of 53.2° (Roche Méane; Supplementary materials Fig. S1).

These 48 events are combined with the *RockTheAlps database* of the Interreg Project (*www.alpine-space.eu/project/rockthealps/*), which is the result of an RSF inventory covering the entire European Alps, in order to provide consistent data to calibrate our propagation model (Sect. 3.2.2) and to complete our data with events propagating on other substrates than glaciers and snow. In this database each RSF event is represented by the topographical profile from the release point up to the tip of the deposit. Here, the known volume is that of the largest single boulder and ranges from 0.02 m^3 to 1000 m^3 for each event. This database is updated annually. In our study, we use 3497 RSF events with heterogeneous volumes that propagated over all types of substratum and environment (forest, meadows, bedrock, *etc.*).

3.2 Mapping release and propagation areas at regional scale

3.2.1 Mapping potential release areas at a regional scale

Statistical analysis of RSF triggering conditions

The *MBM RSF database* is used to analyse the triggering conditions of RSFs according to the predicted MARST and the slope values. The slope is extracted from the 25-m resolution DEM; altitude and aspect are not added to the analysis because they are accounted for by the MARST values through the MAAT and PISR variables. Even if DEMs with better resolution exist locally in the MBM, we choose to keep the IGN DEM at 25m resolution in order to remain consistent with the DEM used to work on a regional scale. Thus, among the 1389 RSFs of the *MBM RSF database*, only the events on the French side of the

massif are kept in the analysis because of low accuracy of the IGN DEM on the Italian side: 984 RSFs are used to determine permafrost conditions, and 1024 for slope conditions – a difference explained by the fact that the SAFRAN meteo data used for the predicted MARST map do not have exactly the same extent as the DEM on the French side of the border (Fig.3).

The *MBM RSF database* allows the distribution of RSFs to be analysed according to their relative frequency, *i.e.* the ratio between the number of RSFs per slope and per predicted MARST class and the rockwall surface area of each slope and of each predicted MARST class. The results of the statistical distribution of RSFs allow the topographic (slope) and permafrost (MARST) conditions the most likely to trigger RSFs to be determined.

Mapping the release areas

The analysis of the *MBM RSF database* is used to set up a multi-criteria GIS scheme to map potential release areas. We first look at the topographical conditions where RSFs are triggered, especially the minimum slope angle required (Fig. 4). The statistical analysis shows that 93.2% of the RSFs occurred on slopes > 30°. 68% of the RSFs are triggered at slope angles between 40° and 60°, while the number of RSFs in relative frequency - *i.e.* normalised by the surface area of each slope class - increases with the slope angle. However, 70 RSFs (6.8%) occurred on slopes < 30°, of which 56 are on crest lines or rockwall bases smoothed by the DEM. The other 14 were triggered in recently deglaciated areas which are still considered as glaciated by the DEM whose data were acquired between 2009 and 2011. Since these outliers result from DEM limitations, we chose to ignore them in our statistical and mapping approach and to consider only the slopes > 30°.

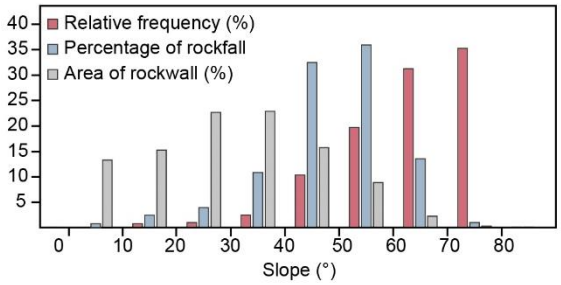

Fig.4 Percentage of RSF by slope class, and relative frequency according to rockwall area

We then calculate the relative frequency of RSFs per predicted MARST class, used to weight the rockwalls according to the intensity of their morphodynamics. Finally, the slope and predicted MARST maps are combined to define a *Rock slope failure Susceptibility Index* (RSI) which displays the permafrost conditions (MARST) that are the most likely to trigger RSFs. We classify the RSIs in three levels based on predicted MARST classes and their respective relative frequency of RSFs. These RSI levels are implemented in a GIS to map different scenarios of potential release areas throughout the French Alps.

3.2.2 Mapping propagation areas at a regional scale

Statistical analysis of RSF propagation characteristics

The propagation of each RSF of the *High Mountain database* and *RockTheAlps database* is characterised by the statistical relation between the Energy Line Angle (ELA) and the Area Under the Profile (AUP). The ELA principle was first described by Heim (1932), who showed that the total travel distance of a falling rock can be described by an imaginary energy line that connects the RSF release zone with the stopping point of the fallen block. The AUP is an index used in hydromorphology (Demoulin 1998) based on the normalization of the water stream longitudinal profile. It has been adapted to help characterise the topographic profiles of RSF events (Colas et al. 2021; Menk et al., 2023). This adaptation consists in scaling the vertical dimension of the profile according only to the total height difference (H0) and the horizontal dimension to the profile length (L_0). In our study, it corresponds to the area under each dimensionless topographic profile (Fig. 5). It is calculated horizontally at a point of altitude z_i and related to the total height difference up to this point according to eq. (1).

$$AUP_i = \frac{\sum_{z_0}^{z_i}(z_{j-1} - z_j) \times (x_j - \frac{(x_j - x_{j-1})}{2})}{(z_i - z_0)^2} \qquad (1)$$

The calculation of the AUP allows different topographic profiles to be compared at the same scale, with their altitudes all varying between 0 and 1 due to the dimensionless process used. This method has the advantage of preserving angles and slopes.

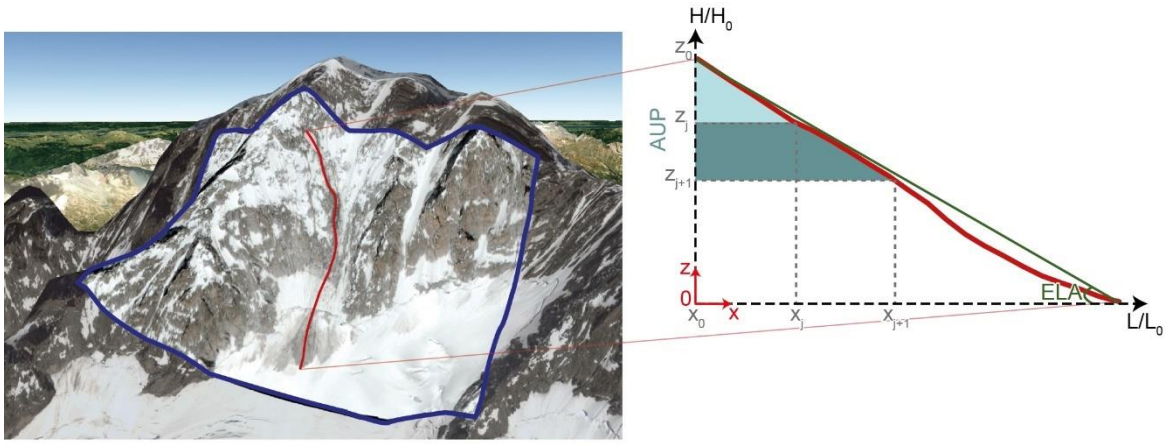

Fig.5 Method used to calculate ELA and AUP. The red line corresponds to the profile of the RSF (measured from the IGN DEM), the blue line corresponds to the contours of the satellite image used to manually digitize the RSF profile

Mapping propagation areas at the regional scale

We implement the normalised area dependant energy line in a simple statistical model (*RockavELA*) to map the potential propagation areas of RSFs at a regional scale. The program is written in C++ using the Qt framework under LGPLv3 license for the entire graphical interface and using OpenMP directives for the parallelization of calculations. It currently runs only on Windows (versions 7 and higher). The software can be download there: https://www.ecorisq.org/publications/software/70-rockavela-install.

The calibration of the model relies on statistical analysis of several propagation processes. Despite it is not based on a physical approach, it can effectively simulate deposition areas. Within the model, numerous virtual trajectories are generated and their simulation follows an iterative process. For each iteration, a value of direction change is first calculated and the virtual trajectory iteration corresponds to an increase of a length defined by the parameter "Segment length" in a direction calculating using the direction change. The direction of the virtual trajectory iteration is generally applied in the direction of the aspect (slope orientation) of the underlying cell except for the first iteration where the direction change is random towards the left or right side of the fall direction, which equals the slope orientation before the first direction change. It is worth noting that the direction change is limited to a *Maximum deviation angle.* After each virtual trajectory iteration, the AUP of the profile corresponding to the virtual trajectory is calculated. For this calculation, the profile is discretised with a resolution defined by the parameter "Profile Step". The virtual propagation stops when an ELA threshold according to AUP given by equation 3-4-5 (depending on the propagation limits) is reached. One can note that the aspect for each cell in the DEM, required for the simulation process, is calculated using the 4 neighbouring cells, following the approach of Zevenbergen, L.W. and Thorne, C.R. (1987).

RockavELA uses the following parameters to model the propagation areas of the RSFs:

(i) *Number of simulations*: number of virtual trajectories calculated by the model that allows to calculate the whole spectrum of direction change values following the probabilistic approach presentation in Eq. 2.

(ii) *Segment length (m)*: planimetric distance between fall direction changes in an RSF trajectory.

(iii) *Profile step (m)*: distance used to discretise the energy line in order to calculate the AUP of the trajectory. It is the planimetric distance between two interpolation points on the trajectory profile.

(iv) *Maximum deviation angle (°)*: the maximum angle of deviation of the virtual trajectory in the RSF trajectory after completing the defined *segment length*. The angle of deviation is sampled between 0 and $angle_{max}$.

The angle of deviation is calculated following the eq. 2:

$$\boldsymbol{angle_{max} \times rand^{2.85}} \quad (2)$$

Where rand is a random number between [0 and 1]

Deviation from the fall direction is always in the direction of the aspect in the cell. The slope of the cell is not considered in the calculation.

(v) *Propagation limit*: allows average or extreme stopping distances to be chosen. This parameter is controlled by a logistic regression to obtain a 10^{-n} occurrence probability of an ELA value in each AUP class calculated from the *Propagation database* (Section 4.2.1). This is therefore observed data that is representative of the reality of the dispersion of phenomena in similar topographical conditions. The statistical analysis is carried out with an interval of 0.01 AUP. Within each interval, only those with a minimum population of 30 events are retained, and this population is used to perform the logistic regression. The equation of the logistic regression for each

propagation limit is given in eq. (3-4-5). These propagation limit are chosen following the MEZAP recommendation about rock hazards (Colas et al. 2022):

- High propagation limit ($\log10^{-6}$):

$$ELA = -15.63 \times \ln(AUP) + 18.872 \quad (3)$$

with AUP [0; 0.07]; ELA = 60.44

- Medium propagation limit ($\log10^{-4}$):

$$ELA = -16 \times \ln(AUP) + 19.647 \quad (4)$$

with AUP [0; 0.07]; ELA = 62.20

- Low propagation limit ($\log10^{-2}$):

$$ELA = -16.83 \times \ln(AUP) + 21.158 \quad (5)$$

with AUP [0; 0.07]; ELA = 65.91

The output of the model is a raster map providing an output called "reach susceptibility" for each cell. The reach susceptibility is calculated as ratio between the number of virtual trajectories that travel through the cell divided by the number of releases from a given release area performed during the modelling. Thereby, all RSFs trajectories from one given release area are modelled using probabilistic approaches combined with algorithms that detect all downslope neighbours from a given cell in a DEM. The reach susceptibility serves as a useful indicator for identifying preferred runout path. It should be used only to determine the concentration of virtual trajectories, and not be interpreted in quantitative aspects.

Calibration of *RockavELA* settings and output evaluation

The calibration and evaluation of *RockavELA* are carried out using the 20 RSF events in the *High Mountain database* for which the satellite images allow a detailed geometrical reconstruction of the propagation areas. 11 of these events are randomly selected for the calibration of *RockavELA* and the 9 others are used for its evaluation. Then we run *RockavELA* for each of these events, with the assumption that the observed propagation areas are associated with medium propagation limits. From these events, the difference in frontal and lateral error between the modelled and the real propagation area is calculated. We suppressed the cells with reach susceptibility values < 1 % from the modelled propagation area since the zones with reach susceptibility < 1% globally corresponded to individual virtual trajectories which had to be suppressed to provide an homogeneous deposition zone. The frontal error is measured by calculating the length difference between the real deposit and the modelled one. This distance is then normalised to provide a percentage error of the modelled deposit compared with the length of the actual deposit (Fig. 6A). The parameters are calibrated to obtain the best travel distance (i) by adjusting the *profile step* parameter from 1 to 2 with a step of 0.1, and (ii) by testing the effect of the *segment length* between 5, 10 and 25 m with a medium propagation limit. Each run is performed with 100 iterations. Once the best fit is obtained, we calibrate the lateral spread by setting the *maximum deviation angle* and *segment length* while maintaining the same *profile step* value. The lateral error is calculated as the difference between the modelled propagation surface area and the actual propagation surface area by

cutting the propagation raster at the front of the shortest deposit (modelled or actual) in order to exclude the frontal error which is already set (Fig. 6B). Only the runs with the best fitting are retained for the regional mapping.

The evaluation of the model is carried out with the low and high propagation limits, which are used for the regional mapping, and the medium scenario. The same error calculation approach used for the model calibration (Fig. 6) is applied for the model evaluation.

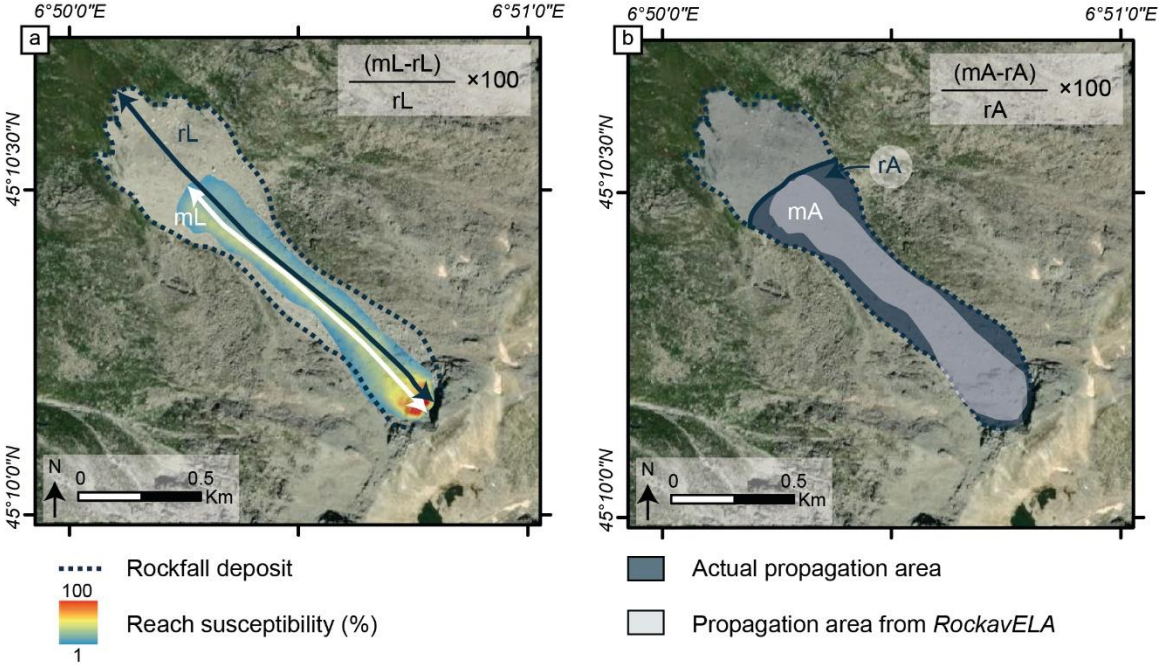

Fig.6 a: Method for measuring frontal error, where mL is the modelled deposit length; rL is the length of the actual deposit with an event used for the validation. b: Method for measuring lateral error, where mA is the modelled deposit area and rA the actual deposit area. (Aerial image source: Esri, Maxar, Earthstar Geographics and the GIS user Community; 2021)

4 Results

This section presents the results of the analysis of RSF triggering conditions and the maps of potential release areas (Sect. 4.1). We then present the propagation characteristics analysis of the events of our databases, the calibration of *RockavELA*, and the resulting propagation area maps (Sect. 4.2).

4.1 Release area mapping

4.1.1 Analysis of RSF triggering conditions according to MARST

The analysis of the RSF distribution according to the predicted MARST is shown in Figure 7. 95% of the RSFs occur in rockwalls with predicted MARST between -4°C to 4°C and more than half of the RSFs (66%) occur between -2 and +2°C. The relative frequency shows a peak of occurrence in rock faces with predicted MARST between -2 and 0°C, with 325 RSFs

(35%) triggered in the 8% of rockwall surface area corresponding to this temperature class. More generally, most RSFs occur between -8°C and +6°C, with only 1.4% of them in predicted MARST ranging between +4 to +6 °C.

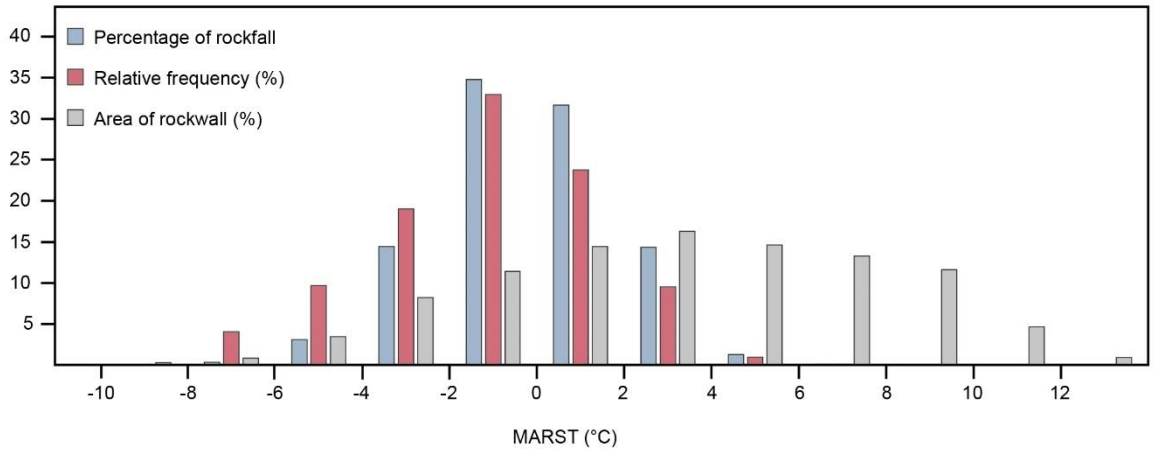

Fig.7 Percentage of RSFs by predicted MARST class, and relative frequency according to rockwall area for each predicted MARST class

4.1.2 RSI levels definition and release areas scenarios

Three RSI levels are determined to propose different release area scenarios according to the relative frequency of RFSs for the various predicted MARST classes (Fig. 7 and 8) as follows:

- RSI 1: The first scenario is a conservative one and preserves a maximum of rockwalls in which > 98% of the RSFs are triggered. It concerns all rockwalls whose predicted MARST ranges between -8°C and +4°C.
- RSI 2: The second scenario is a medium one in which > 80% of the RSFs are triggered and whose predicted MARST ranges from -4 °C to +2°C.
- RSI 3: The third scenario corresponds to the rockwalls with the highest relative frequency and groups the rockwalls whose predicted MARST ranges from -2°C to +0°C.

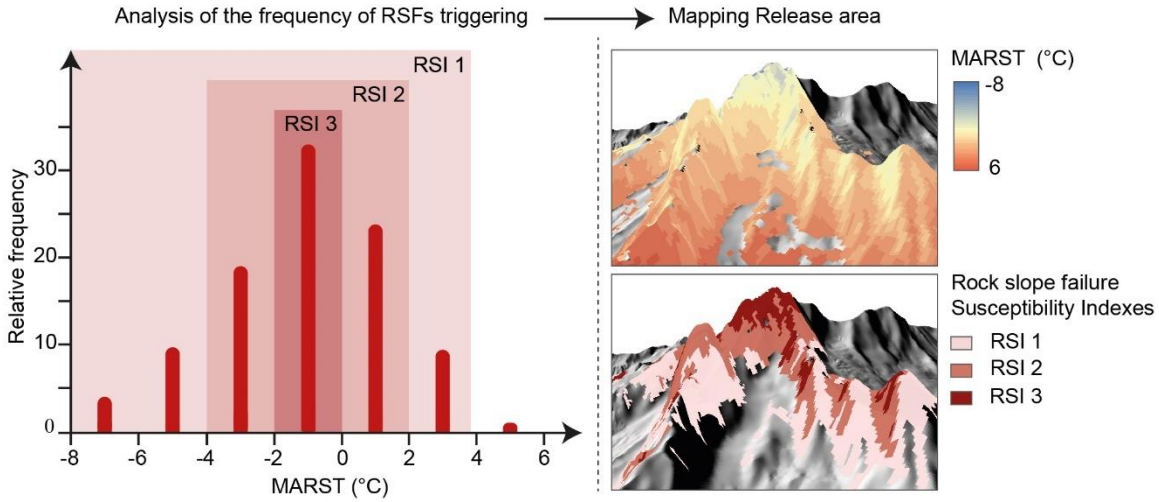

Fig.8 Definition of the RSI according to the relative RSF frequency by predicted MARST classes, and an example in the Aiguille Verte and Drus sector (MBM)

4.1.3 Release area maps

The release area maps show that 284 km² of the French Alps could be considered as sectors in which RSFs may be triggered under a conservative scenario (RSI 1), 112 km² with the medium scenario, and 34 km² with the scenario considering only the most active rockwalls (RSI 3). The detailed results for each zone of the French Alps as displayed in Figure 1 are given in Table 1.

	RSI 1		RSI 2		RSI 3	
	Area (km²)	Rockwall (%)	Area (km²)	Rockwall (%)	Area (km²)	Rockwall (%)
Zone 1	24.6	8.3	20.6	6.9	9.6	3.2
Zone 2	136.1	9.8	55.0	4.0	14.5	1.0
Zone 3	80.7	6.0	29.4	2.2	9	0.7
Zone 4	42.2	2.5	7.3	0.4	0.4	0.0
French Alps	**283.6**	**6**	**111.8**	**2.4**	**33.5**	**0.7**

Table 1. Surface area covered by the three RSI levels for each zone of the French Alps. The percentage of rockwall corresponds to the surface affected by the RSI in rockwalls above 1500 m.a.s.l. As the RSIs do not extend below 1500 m a.s.l, the percentages in this table only consider the rockwalls > 1500 m a.s.l to be representative of the periglacial environments studied here

The proportion of RSI 3 is more important in zone 1 (northernmost ranges) compared with the other zones. In contrast, zone 4 (southernmost range) is marginally affected by potential release areas, even under RSI 1, which can be explained by a less extensive distribution of permafrost in the Southern Alps.

An example of the RSI in the MBM is shown in Figure 9, the other zones are given in Supplementary materials Fig. S4-7.

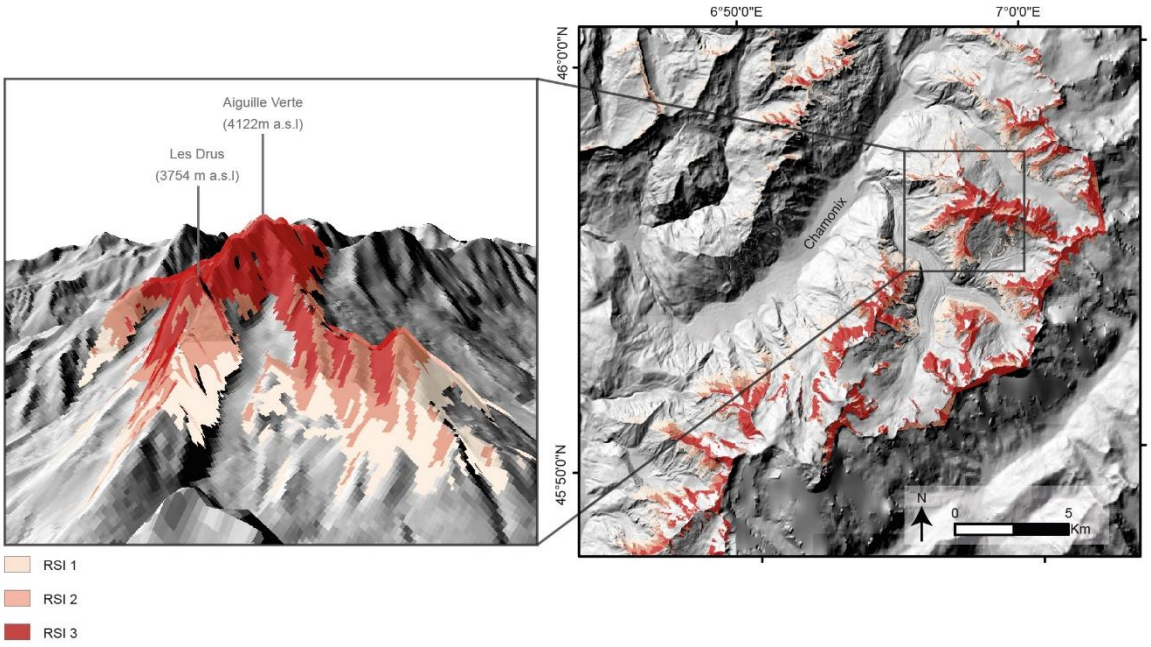

Fig.9 Example of the three levels of RSI in zone 1 (MBM and Aiguilles Rouges massif) with a focus on the Aiguille Verte and Drus area

4.2 Propagation area analysis and mapping

4.2.1 RSFs propagation characteristics analysis

The comparison between the propagation characteristics of the 48 events in the *High Mountain database* with those in the *RockTheAlps database* shows that they all follow the same distribution, regardless of their volume, their lithology, or the substrate on which they travel (Fig. 10). The analysis of the Propagation databases do not show a link between ELA and volumes, at least for the range of volumes represented in our database. We therefore decided to merge these two databases to form the *Propagation database*, from which we propose three propagation limit according to the logistic regressions proposed in Sect. 3.2.2. The analysis of the Propagation databases do not show a link between ELA and volumes, at least for the range of volumes represented in our database (Supplementary materials Fig. S8)

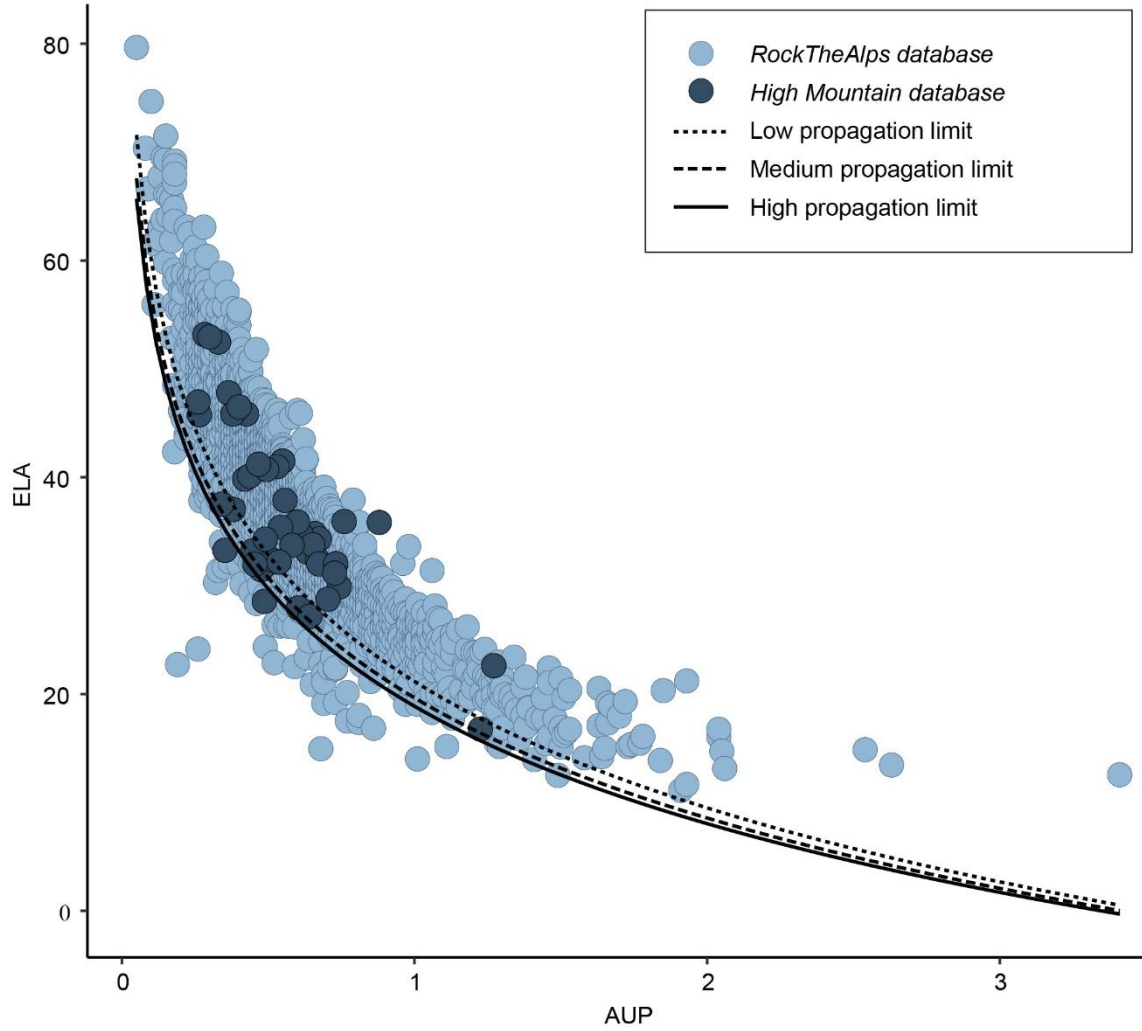

Fig.10 ELA *vs.* AUP for the *RocktheAlps database* and the *High Mountain database* events. The three propagation limit correspond to the logistic regressions chosen in *RockavELA (described in section 3.2.2)*

4.2.2 Calibration results of *RockavELA*

Frontal error

In order to calibrate the runout distance, we adjust the *segment length* and *profile step* settings with the medium propagation limit proposed in *RockavELA*. The most successful results are obtained with a *profile step* of 1.1 m regardless of the *segment length* chosen (25, 10, or 5 m). In each case, 50% of the modelled RSFs have a frontal error between -25 and 25%, and a median value very close to 0% (Fig. 11). The details of the frontal error for each run of the calibration are given in Supplementary materials Fig. S9.

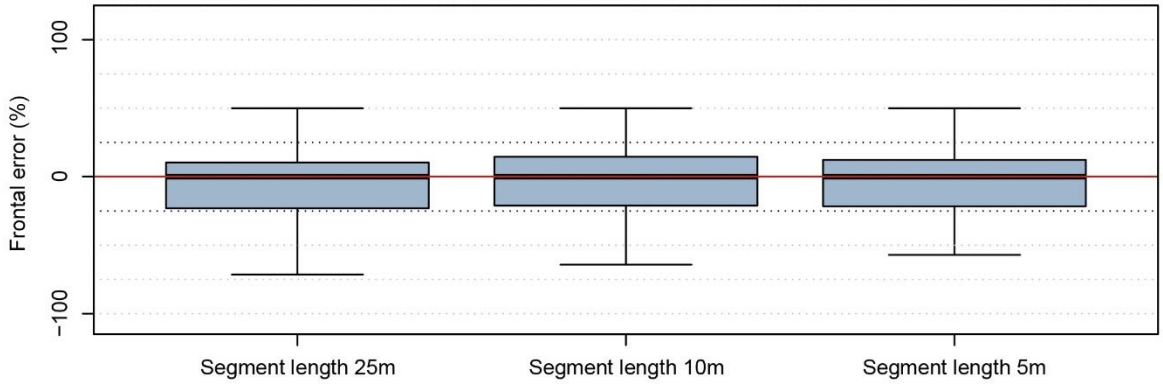

Fig.11 Percentage of frontal error with the best settings selected to calibrate the runout distances in *RockavELA* (1.1 m profile step; medium propagation limit)

Lateral error

The lowest lateral errors are obtained with a *segment length* of 5 m and a *maximum deviation angle* of 10°. With these parameters, almost 50% of the RSFs have a lateral error between -11 and 52%, and a median close to 15% (Fig. 12). This setting provides the smallest lateral error. However, the width of the modelled deposit is sometimes overestimated and three of the collapses have an error exceeding 50%. The details of the results according to the *segment length* and the *maximum deviation angle* chosen to analyse the results are given in Supplementary materials Fig. S10.

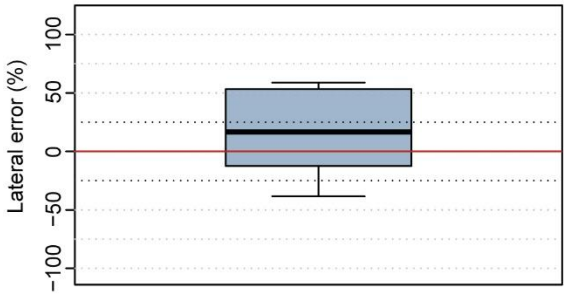

Fig.12 Percentage of lateral error with the best setting retained to calibrate lateral spreading in *RockavELA* (*segment length* 5 m, profile step 1.1 m, *maximum deviation angle* 10° and medium risk acceptance)

Considering the results obtained in the calculations of frontal and lateral errors of *RockavELA*, we choose to retain the following settings for the mapping at regional scale:

- First we use a 5 m *segment length* with a *maximum deviation angle* about 10° to control the lateral spreading.
- Then we use a 1.1 m *profile step* to adjust the runout distance.

4.2.3 *RockavELA* output across the French Alps

This section shows the results of *RockavELA* simulation in the French Alps with, as release areas, the sectors corresponding to RSI 2. Considering all the sectors with a reach susceptibility ≥ 1%, 586 km² of terrain could be reached by RSFs with a high

propagation limit and 472 km² with a low propagation limit. For the entire French Alps, the difference of surface area between the low and high propagation limits represents 24% with a reach susceptibility ≥ 1%. The detailed spatial analysis of the results for each zone is given in Table 2.

	Zone 1	Zone 2	Zone 3	Zone 4	French Alps
	Area (km²) with a reach susceptibility *≥ 1%*				
High Propagation limit	110	232	213	31	586
Low Propagation limit	90	183	174	24	472
Difference (%) of area between low and high propagation scenario	22	26	23	27	24

Table 2 Areas (in km²) that can be reached by RSF in the entire French Alps and in each zone; and the difference (in %) of area between high and low propagation limit

Figure 13 shows an example of the *RockavELA* output with RSI 2 as release areas and a low propagation limit in the MBM. The propagation maps of all the simulations are given in Supplementary materials Fig. S11-18.

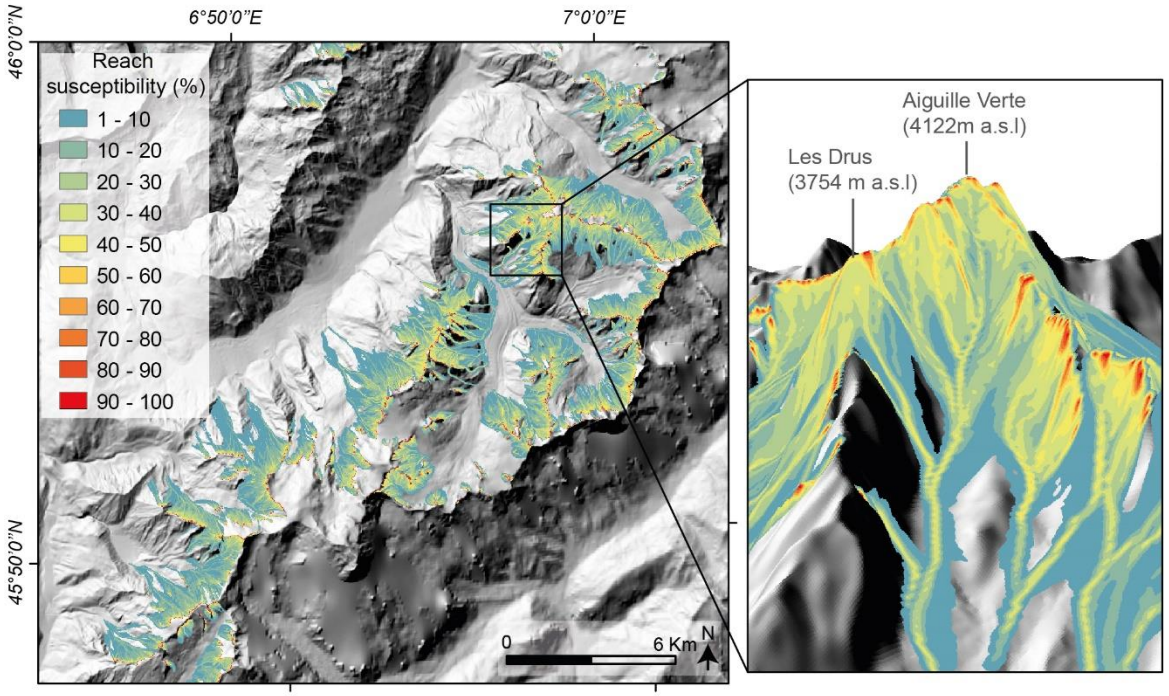

Fig.13 Sectors that could be reached by potential RSFs in the MBM according to *RockavELA* output with a low-propagation limit, and a focus on the Aiguille Verte and Drus sector

4.2.4 Evaluation of the propagation area maps

The model evaluation shows consistent frontal and lateral errors between the actual and modelled deposits. Indeed, it can be observed on Figure 14-A that the frontal error remains between -25 and +25% for 50% of the RSFs with high and medium propagation limit. With the low propagation limit, the frontal error ranges between -38% and 0% for half of the sample.

435 Concerning the evaluation of the lateral error, we can see on Figure 14-B that the results are consistent. Indeed, the difference between the modelled lateral spread and that of the real deposits stays between -25 and +25% for almost 50% of the sample.

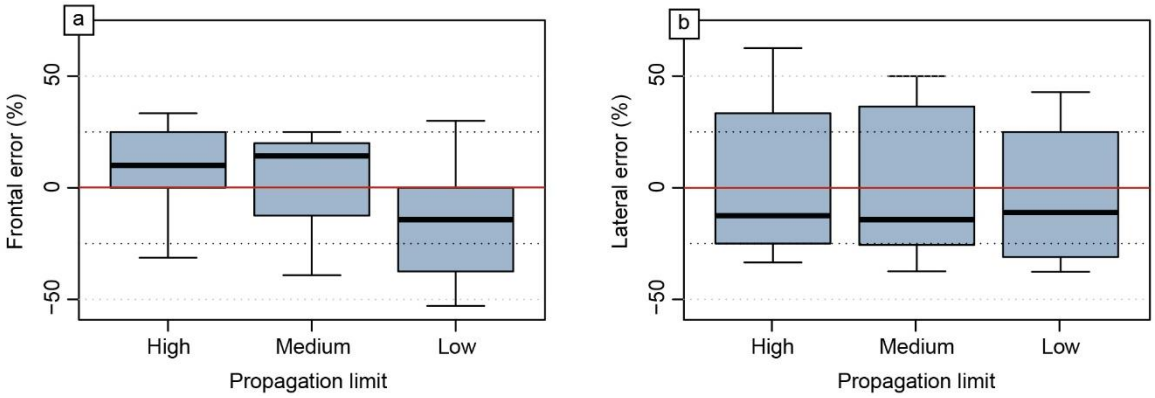

Fig.14 a: Percentage of frontal errors with the best settings used for the evaluation of *RockavELA*. b: Percentage of lateral errors with the best settings used for the evaluation of *RockavELA*.

5 Discussion

440 ### 5.1 Release area mapping: interpretation and limits of the approach

The mapping of the release areas proposed here provides a first overview of the susceptibility to RSF triggering according to the permafrost conditions in the French Alps. The robustness of the approach used in this study relies on a unique database which gives the first overview of the permafrost-affected rockwalls the most prone to RSF triggering. It is worth noting that the analysis highlights the strong link between permafrost and RSFs. Indeed, permafrost is expected at MARST reaching up

445 to 3°C according to Hasler et al (2011b), and 98.6% of RSFs have occurred from rockwalls with predicted MARST ≤ 3°C. But it is also interesting to note that the most active rockwalls are those with warm (close to 0°C) permafrost, confirming other databases analyses (*e.g.*, Knoflach et al. 2021) and laboratory tests. The latter show that frozen rock may become particularly unstable when ice-filled fractures warm towards the melting point (*e.g.*, Davies et al. 2001; Mamot et al. 2018). Other studies have also shown that expected cold permafrost conditions may become unstable due to water infiltration and accelerated cleft-

450 ice erosion (Hasler et al. 2011a), which can explain RSF events under MARST < -2°C.

The definition of RSI levels according to the distribution of RSF by predicted MARST classes allows 3 more or less conservative scenarios of release areas to be proposed. However, it is possible to adjust these levels to propose other scenarios according to the use of the maps. Our approach that accounts for slope and permafrost conditions does not include other

parameters which also affect rockwall stability such as the geological structure, lithology, local discontinuities (*e.g.*, fault, joints, foliation; Stead et al. 2015), and glacial history (McColl 2012; McColl and Draebing 2018) that also affect the thermal properties and dynamics of the rock (Wegmann et al. 1998; Hasler et al. 2011a; Magnin and Josnin 2021) as well as their mechanical behaviour (Etzelmüller et al. 2022). Moreover, as the MBM lithology is relatively homogeneous (granite and gneiss), the *MBM RSF database* is not representative of the lithology of the other massifs of the French Alps, or their geological and glacial evolution. Nevertheless, the 5 RSFs of the *High Mountain database* that are outside the MBM, are also located in the release area maps (two are in an area with RSI = 1; two are in RSI = 2 and one in RSI= 3). The compilation and analysis of larger databases in the high mountain environments could therefore improve the release area maps proposed in this study by including structural and lithological effects in RSF triggering (Stead et al. 2015; Blondeau et al. 2021).

Another limitation of this work is relative to the DEM resolution which smooths the slopes, especially in the vicinity of crest lines. These ridges are sometimes not considered by the release area mapping, which only considers slope angles > 30°. However, this artefact does not influence the propagation areas modelled in the Section 4.2. Moreover, the DEM is built upon data acquired during 2009-2011, but since then, glaciers have retreated and have sometimes exposed steep slopes and moraines which do not appear in the release area maps of this study. Therefore, interpretation of the release area maps at the local scale must consider this limitation.

Despite the limitations at local scale, our study based on a unique and large database is consistent at regional scale to provide a first overview of the permafrost-affected rockwalls prone to destabilisation in the whole French Alps. The proposed method for mapping release areas could serve as a baseline for future applications in this range or other permafrost-affected high mountain ranges of the world. However, it remains essential to submit the release areas maps to expert approval for a better a better interpretation at site scale.

5.2 Limitations and guidelines for the use of *RockavELA*

For this study, we specifically developed a new propagation model, *RockavELA*. Other models have been developed to map regional zonation of rockfalls (Dorren 2003; Li et Lan 2015), but they are not specifically used for the high mountain environments or for events with heterogeneous volumes such as those we are investigating in this study. Some approaches are appropriate for events travelling onto glaciers (*e.g.*, Noetzli et al. 2006; Sosio et al. 2012) but are developed for high magnitude events such as large rock-ice avalanches. Other studies propose GIS approaches based on flow direction from DEM to model propagation areas (D8 or D16 algorithm; Huggel et al. 2003), but this method tends to channel the flows or to spread them too much, depending on the chosen algorithm. Other works use multiple hazards assessment (Gruber and Mergili 2013; Horton et al. 2013) or multiple phase mass flow models for process chains (Mergili et al. 2017) but these models are often used at the scale of the catchment or the region (e.g., Mergili et al. 2019), but rarely for larger scales such as the French Alps. These complex models require a greater amount of input data (such as volumes, material density, rheology parameters, etc.) that are not available or cannot be generalised to the scale of the French Alps. In our study, we developed *RockavELA* to map the propagation areas of RSFs on a regional scale, a simple model that is easily run on the whole French Alps using the

dimensionless area-based energy line principle, and requires as input data only a DEM and release areas. The real robustness of our approach relies on the setting, the calibration and the evaluation of the model, which are performed with a unique RSF database (P*ropagation database*) that is highly representative of the propagation characteristics of RSFs. This is also one of the first studies that proposes to quantify the frontal and lateral error propagation areas with the comparison of the model outputs and the actual events from our databases.

However, one of the limitations of the method used to calibrate the model could be related to the small number of events in the *High Mountain database* for which we have precise satellite images to study the morphology and geometry of the deposit. But interestingly, these events, which mostly occurred in high mountains with specific substrate (mostly glacier and snow), corroborate the propagation characteristics of the *RockTheAlps database* despite a wider range of volume and runout substrate. The diversity of the 3497 events in the *RockTheAlps database* (in terms of volumes, substrates, altitudes, etc.), and its enrichment with the 48 events from the *High Mountain database* mean that the proposed setting is reproducible in other mountain ranges. If the *Propagation database* shows no effect of lithology and volume on the observed propagation lengths (Supplementary materials Fig. S8), it must be kept in mind that above a certain volume, rock avalanches tend to propagate much further, especially in glaciated environments (Noetzli et al. 2006). Therefore, *RockavELA* could also be re-calibrated and re-evaluated using other databases (*e.g.*, Knoflach et al. 2021) and other settings could thus be considered to run the propagation model.

Despite the calibration and the setting based on the propagation characteristics of our databases, the remaining frontal error (< ±25% in most of the cases) and a lateral error (< ±50%) in the evaluation of the results could be explained by the lack of consideration for complex dispersion processes involving factors such as the type of substrate, the lithology of the falling rock and its fragmentation at local scale (Lan et al. 2022). However, this locally observed range of error remains sufficient for a preliminary assessment at a regional scale. Similarly to the release area maps, the limitations in the extents of the propagation areas must be considered for interpretation of the maps at the local scale.

In addition to the parameters that directly control the stopping distance and the spread of the RSF trajectories in *RockavELA*, the model is also sensitive to the DEM resolution. For example, as it smooths the slopes and underestimates the steepness, some artefacts can be generated in the simulated runout areas when release areas are situated on a crest line, with RSF trajectories following the crest line instead of running along the slopes (Supplementary materials Fig. S19). When testing the simulations with a 0.2-m resolution DEM resampled at 5, 10 and 25 m, the artefacts disappear with the 5 m one but not with the 10 and 25 m, meaning that the model is sensitive to the DEM resolution and not just its accuracy. However, runout pixels affected by these artefacts are marginal with reach probabilities that are typically very low. Indeed, it disappears above a 5% reach susceptibility with a 25 m DEM, a 2% reach susceptibility with a 10 m DEM and a 1% reach susceptibility with a 5 m DEM (Supplementary materials Fig. S19). Therefore, we could recommend using a higher DEM resolution for implementing *RockavELA*, which does not exist for the French Alps.

Otherwise, beyond 100 iterations, we observe no significant influence on the runout distance or lateral spread of the modelled propagation areas. We therefore choose to keep 100 iterations, which is a compromise between calculation time and robustness of the results.

For a more robust interpretation of the propagation maps, we should avoid interpreting reach susceptibility in quantitative terms, and instead consider all the areas > 1% as a potentially reachable area. The reach susceptibility value only indicates the concentration of preferred virtual trajectories. The choice of the reach susceptibility threshold depends on the expert knowledge and could be adjusted according to the use of the maps. However, we have chosen to keep the reach susceptibility values from 1 to 100% in this study, especially for the calibration and evaluation of the model, to measure the length and area of each RSF deposit in order to consider the entire modelled trajectories.

Considering these different observations, the use of *RockavELA* in the risk analysis context should be submitted to expert knowledge to avoid an over-simplified interpretation of the results.

5.3 Future applications

This work characterises and maps the potential release and propagation areas of RSFs on a regional scale in order to highlight potential hot spots that could be reached by RSFs.

Comparing these maps with human concerns (*e.g.*, infrastructure, mountaineering routes) could allow a preliminary assessment of those at risk of RSF impact. This is an essential step in permafrost hazard assessment for evaluating and anticipating the future risks, particularly in the current context of permafrost degradation (GAPHAZ 2017). Following this preliminary identification, in-depth studies on a local scale could be carried out to get a better estimation of the trajectories but also mobility parameters of potential RSFs with physics-based models (*e.g.*, Bartelt et al. 2018) or with RSF monitoring to better assess the dynamics of the considered source area. For example, the first results from this work point out some highly frequented areas, such as the normal route to the Mont Blanc (Fig. 15), that is already known as a highly hazardous area (Mourey et al. 2022). This example thus confirms the ability of our mapping approach to identify potential hot spots which could merit more in-depth analysis at the local scale for better risk assessment and mitigation.

Another possible application of our study could be to implement it in other mountain ranges. Since the calibration of our model is based on unique and consistent databases, and many other mountain ranges are experiencing an increase in RSF activity from permafrost-affected rockwalls that prompts urgent identification of potential areas at risk (Allen et al. 2022), a preliminary assessment could be conducted with such an approach.

This work could also be applied with consideration of future permafrost degradation and glacier retreat, implying an altitudinal shift in the permafrost lower limit and exposure of steep, unstable deglaciated slopes by applying the expected air temperature change to the predicted permafrost map (Penna et al. 2023).

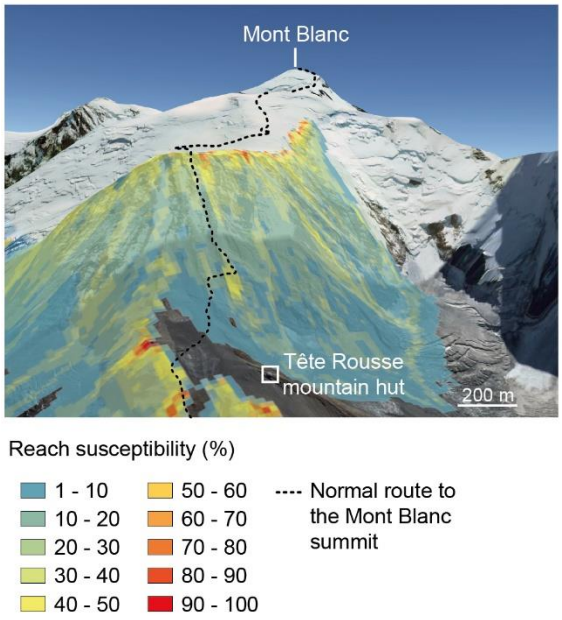

Figure 1 : Classic route to the Mont Blanc (4808 m a.s.l.) which crosses potential propagation areas modelled with *RockavELA* (RSI 2; low propagation limit).

6 Conclusions

This study proposes the first assessment in the French Alps of permafrost-affected rockwalls favourable to RSF triggering and their potential propagation areas using unique and extensive RSF databases. Three RSF susceptibility indexes (RSI) are proposed, based on the level of RSF activity according to predicted permafrost (Mean Annual Rock Surface Temperature; MARST) conditions. These RSI are then used to map three release area scenarios, encompassing more or less active permafrost-affected rockwalls. The resulting maps are used as input for a simple propagation model (*RockavELA*) developed in order to map the propagation areas. Three propagation limit are proposed in this study, defined using propagation characteristics of 3545 events (*Propagation database*), with 48 events occurring in high mountain environments (*High Mountain database*) and 3497 events from lower areas (*RockTheAlps database*).

Analysis of the different RSF databases and release areas and propagation area mapping leads to the following conclusions:

- Analysis of 1389 RSFs inventoried in the MBM between 2007 and 2019 reveals that 95% of the RSFs occurred in rockwalls with predicted MARST between -4°C to 4°C and 66% between -2 and +2°C. This finding highlights the strong link between RSFs and permafrost, and notably with warm permafrost conditions.
- The 3 levels of RSI suggest that release areas could be as extensive as 284 km² (RSI 1; most conservative scenario) but are restricted to 34 km² when considering only the most active rockwalls (RSI 3).

- The *Propagation database* analysis reveals that the 48 RSFs occurring in high mountains environments (*High Mountain database*) and 3497 events from lower altitudes (*RockTheAlps database*) have the same propagation characteristics, despite the heterogeneity of their volume or their travelling substrate.
- We propose three propagation limits allowing different levels of propagations stopping distance. This parameter is controlled by logistic regressions to obtain a 10^{-n} occurrence probability of an ELA value in each AUP class calculated from the *Propagation* databases.
- When calibrating the modelled propagation areas against 11 observed RSFs, our best-fit solution results in frontal error (runout distance) < ± 25% for half of the events and < ± 50% for all the RSFs observed. Lateral error (lateral spread of the deposit) hardly exceeds ± 50% of the observed extent of the deposits. It would be of great interest to work further on this calibration by expanding our databases with more events for which we have accurate information on the propagation areas.
- Evaluation of the output maps by comparing the propagation areas with 9 observed RSFs shows that frontal and lateral errors hardly exceed ± 50% of the observed extent of the deposits whatever the chosen propagation limit.
- The propagation area maps suggest that under RSI 2, RSFs in the French Alps could reach 472 km² with a low propagation limit and 586 km² with a high propagation limit. The extent of potentially reachable areas has limited sensitivity to the propagation limit. Indeed, the difference in surface areas that can be potentially impacted by RSFs between the lower and the higher scenario is < 25 %.
- Sensitivity analysis to the DEM resolution shows that the propagation area maps are sensitive to the DEM resolution and that artefacts can occur with rather coarse resolution, such as the one we use for our study. Higher resolutions are thus recommended for a better assessment of propagation areas to avoid these artefacts that may affect the local interpretation.

The release and propagation area maps could be a first step to highlight potentially hazardous areas and to identify potential human assets (mountaineering routes, high mountain infrastructure, tourism areas) and factors of cascading hazards such as lakes that could be impacted by RSFs. This approach must be considered as a preliminary step to identify hot spots before conducting more in-depth analysis at the local scale. Results must therefore be subject to critical review and confirmation by an expert, and such studies would benefit from comparison with other datasets to improve the definition of potential release areas and propagation limit. Similar approaches could be conducted on other mountain ranges affected by increasing RSF activity from permafrost-affected rockwalls, and regional assessment is an area of growing interest in the context of permafrost degradation.

References

Allen S, Frey H, Haeberli W, et al (2022) Assessment Principles for Glacier and Permafrost Hazards in Mountain Regions. In: Oxford Research Encyclopedia of Natural Hazard Science. https://oxfordre.com/naturalhazardscience/view/10.1093/acrefore/9780199389407.001.0001/acrefore-9780199389407-e-356. Accessed 2 Feb 2022

Allen S, Frey H, Huggel C (2017) Assessment of Glacier and Permafrost Hazards in Mountain Regions. Technical Guidance Document

Auer I, Böhm R, Jurkovic A, et al (2007) HISTALP—historical instrumental climatological surface time series of the Greater Alpine Region. Int J Climatol 27:17–46. https://doi.org/10.1002/joc.1377

Ballantyne CK (2002) Paraglacial geomorphology. Quaternary Science Reviews 21:1935–2017. https://doi.org/10.1016/S0277-3791(02)00005-7

Bartelt P, Christen M, Bühler Y, Buser O (2018) Thermomechanical modelling of rock avalanches with debris, ice and snow entrainment. Numerical methods in geotechnical engineering IX 1047–1054

Bénévent E (1926) Documents sur le climat des Alpes françaises. Étude critique. Revue de Géographie Alpine 14:681–764. https://doi.org/10.3406/rga.1926.5004

Biskaborn BK, Smith SL, Noetzli J, et al (2019) Permafrost is warming at a global scale. Nature Communications 10:264. https://doi.org/10.1038/s41467-018-08240-4

Blondeau S, Gunnell Y, Jarman D (2021) Rock slope failure in the Western Alps: A first comprehensive inventory and spatial analysis. Geomorphology 380:107622. https://doi.org/10.1016/j.geomorph.2021.107622

Boeckli L, Brenning A, Gruber S, Noetzli J (2012) A statistical approach to modelling permafrost distribution in the European Alps or similar mountain ranges. The Cryosphere 6:125–140. https://doi.org/10.5194/tc-6-125-2012

Böhm R, Jones PD, Hiebl J, et al (2010) The early instrumental warm-bias: a solution for long central European temperature series 1760–2007. Climatic Change 101:41–67. https://doi.org/10.1007/s10584-009-9649-4

BRGM (2015) BD Million-Géol: Carte Géologique à 1/1 000 000 Métropole, Image et Vecteur.

Budimir M, Brown S, Sneddon A, et al (2019) Challenges and innovations in operational flood and landslide early warning systems in Nepal, Peru and India. 15881

Byers AC, Rounce DR, Shugar DH, et al (2018) A rockfall-induced glacial lake outburst flood, Upper Barun Valley, Nepal. Landslides. https://doi.org/10.1007/s10346-018-1079-9

Cathala M, Magnin F, Linsbauer A, Haeberli W (2021) Modelling and characterizing glacier-bed overdeepenings as sites for potential future lakes in the deglaciating French Alps. Géomorphologie : relief, processus, environnement 27:19–36. https://doi.org/10.4000/geomorphologie.15255

Colas B, Berger F, Martin R (2021) Guide technique MEZAP. Caractérisation de l'aléa rocheux dans le cadre d'un Plan de Prévention des Risques Naturels (PPRn) ou d'un Porter à connaissance (PAC) des aléas.. BRGM. Collection scientifique et technique. ISBN 978-2-7159-1760-5.

Davies M, Hamza O, Harris C (2001) The effect of rise in mean annual temperature on the stability of rock slopes containing ice-filled discontinuities. Permafrost and Periglacial Processes 12:137–144. https://doi.org/10.1002/ppp378

Deline P, Broccolato M, Noetzli J, et al (2013) The December 2008 Crammont Rock Avalanche, Mont Blanc Massif Area, Italy. In: Margottini C, Canuti P, Sassa K (eds) Landslide Science and Practice: Volume 4: Global Environmental Change. Springer, Berlin, Heidelberg, pp 403–408

Deline P, Gruber S, Amann F, et al (2021) Ice loss from glaciers and permafrost and related slope instability in high-mountain regions. In: Snow and Ice-Related Hazards, Risks, and Disasters. Elsevier, pp 501–540

Demoulin A (1998) Testing the tectonic significance of some parameters of longitudinal river profiles : the case of the Ardenne (Belgium, NW Europe). Geomorphology (Amst) 24:189–208

Dorren L (2003) A review of rockfall mechanics and modelling approaches. Organic Geochemistry - ORG GEOCHEM 27:. https://doi.org/10.1191/0309133303pp359ra

Durand Y, Brun E, Merindol L, et al (1993) A meteorological estimation of relevant parameters for snow models. Annals of Glaciology 18:65–71. https://doi.org/10.3189/S0260305500011277

Duvillard P-A, Ravanel L, Deline P (2015) Risk assessment of infrastructure destabilisation due to global warming in the high French Alps. Journal of Alpine Research| Revue de géographie alpine

Duvillard P-A, Ravanel L, Marcer M, Schoeneich P (2019) Recent evolution of damage to infrastructure on permafrost in the French Alps. Regional Environmental Change 19:1281–1293

Einhorn B, Eckert N, Chaix C, et al (2015) Changements climatiques et risques naturels dans les Alpes . Impacts observés et potentiels sur les systèmes physiques et socio-économiques. Journal of Alpine Research | Revue de géographie alpine. https://doi.org/10.4000/rga.2829

Etzelmüller B, Guglielmin M, Hauck C, et al (2020) Twenty years of European mountain permafrost dynamics—the PACE legacy. Environ Res Lett 15:104070. https://doi.org/10.1088/1748-9326/abae9d

Etzelmüller B, Czekirda J, Magnin F, et al (2022) Permafrost in monitored unstable rock slopes in Norway – new insights from temperature and surface velocity measurements, geophysical surveying, and ground temperature modelling. Earth Surface Dynamics 10:97–129. https://doi.org/10.5194/esurf-10-97-2022

Evans S, Clague J, J. Woodsworth G, Hungr O (1989) The Pandemonium Creek Rock Avalanche, British Columbia. Canadian Geotechnical Journal - CAN GEOTECH J 26:427–446. https://doi.org/10.1139/t89-056

Evans SG, Hungr O (1993) The assessment of rockfall hazard at the base of talus slopes. Can Geotech J 30:620–636. https://doi.org/10.1139/t93-054

Fischer L, Kääb A, Huggel C, Noetzli J (2006) Geology, glacier retreat and permafrost degradation as controlling factors of slope instabilities in a high-mountain rock wall: the Monte Rosa east face. Natural Hazards and Earth System Science 6:761–772

Fischer L, Amann F, Moore JR, Huggel C (2010) Assessment of periglacial slope stability for the 1988 Tschierva rock avalanche (Piz Morteratsch, Switzerland). Engineering Geology 116:32–43. https://doi.org/10.1016/j.enggeo.2010.07.005

Fischer L, Purves RS, Huggel C, et al (2012) On the influence of topographic, geological and cryospheric factors on rock avalanches and rockfalls in high-mountain areas. Natural Hazards and Earth System Sciences 12:241–254. https://doi.org/10.5194/nhess-12-241-2012

Furian W, Loibl D, Schneider C (2021) Future glacial lakes in High Mountain Asia: an inventory and assessment of hazard potential from surrounding slopes. Journal of Glaciology 67:653–670. https://doi.org/10.1017/jog.2021.18

GAPHAZ (2017) Assessment of Glacier and Permafrost Hazards in Mountain Regions - Technical Guidance Document. International Association of Cryospheric Sciences (IASC) and the International Permafrost Association (IPA), Zurich, Switzerland / Lima, Peru. 72 p.

Gardent M, Rabatel A, Dedieu J-P, Deline P (2014) Multitemporal glacier inventory of the French Alps from the late 1960s to the late 2000s. Global and Planetary Change 120:24–37. https://doi.org/10.1016/j.gloplacha.2014.05.004

Gottardi F (2009) Estimation Statistique Et Réanalyse Des Précipitations En Montagne Utilisation D'ébauches Par Types De Temps Et Assimilation De Données D'enneigement Application Aux Grands Massifs Montagneux Français. Institut National Polytechnique de Grenoble - INPG

Gruber S, Haeberli W (2007) Permafrost in steep bedrock slopes and its temperature-related destabilization following climate change. Journal of Geophysical Research: Earth Surface 112:. https://doi.org/10.1029/2006JF000547

Gruber FE, Mergili M (2013) Regional-scale analysis of high-mountain multi-hazard and risk indicators in the Pamir (Tajikistan) with GRASS GIS. Nat Hazards Earth Syst Sci 13:. https://doi.org/10.5194/nhess-13-2779-2013

Guzzetti F, Gariano SL, Peruccacci S, et al (2020) Geographical landslide early warning systems. Earth-Science Reviews 200:102973. https://doi.org/10.1016/j.earscirev.2019.102973

Haberkorn A, Kenner R, Noetzli J, Phillips M (2021) Changes in Ground Temperature and Dynamics in Mountain Permafrost in the Swiss Alps. Frontiers in Earth Science 9:

Haeberli W, Schaub Y, Huggel C (2016a) Increasing risks related to landslides from degrading permafrost into new lakes in de-glaciating mountain ranges. Geomorphology 293:405–417. https://doi.org/10.1016/j.geomorph.2016.02.009

Haeberli W, Buetler M, Huggel C, et al (2016b) New lakes in deglaciating high-mountain regions – opportunities and risks. Climatic Change 139:201–214. https://doi.org/10.1007/s10584-016-1771-5

Hartmeyer I, Delleske R, Keuschnig M, et al (2020) Current glacier recession causes significant rockfall increase: the immediate paraglacial response of deglaciating cirque walls. Earth Surface Dynamics 729–751. https://doi.org/10.5194/esurf-8-729-2020

Hasler A, Gruber S, Font M, Dubois A (2011a) Advective Heat Transport in Frozen Rock Clefts: Conceptual Model, Laboratory Experiments and Numerical Simulation. Permafrost and Periglacial Processes 22:378–389. https://doi.org/10.1002/ppp.737

Hasler A, Gruber S, Haeberli W (2011b) Temperature variability and offset in steep alpine rock and ice faces. The Cryosphere 5:977–988. https://doi.org/10.5194/tc-5-977-2011

Heim A (1932) Bergsturz und Menschenleben. Fretz & Wasmuth

Horton P, Jaboyedoff M, Rudaz B, Zimmermann M (2013) Flow-R, a model for susceptibility mapping of debris flows and other gravitational hazards at a regional scale. Natural Hazards and Earth System Sciences 13:869–885. https://doi.org/10.5194/nhess-13-869-2013

Hsü KJ (1975) Catastrophic Debris Streams (Sturzstroms) Generated by Rockfalls. GSA Bulletin 86:129–140. https://doi.org/10.1130/0016-7606(1975)86<129:CDSSGB>2.0.CO;2

Huggel C, Kääb A, Haeberli W, Krummenacher B (2003) Regional-scale GIS-models for assessment of hazards from glacier lake outbursts: evaluation and application in the Swiss Alps. Natural Hazards and Earth System Sciences 3:647–662. https://doi.org/10.5194/nhess-3-647-2003

Huggel C, Zgraggen-Oswald S, Haeberli W, et al (2005) The 2002 rock/ice avalanche at Kolka/Karmadon, Russian Caucasus: assessment of extraordinary avalanche formation and mobility, and application of QuickBird satellite imagery. Natural Hazards and Earth System Sciences 5:173–187. https://doi.org/10.5194/nhess-5-173-2005

Huggel C, Fischer L, Schneider D, Haeberli W (2010) Research advances on climate-induced slope instability in glacier and permafrost high-mountain environments. Geographica Helvetica 65:146–156. https://doi.org/10.5194/gh-65-146-2010

Huss M (2012) Extrapolating glacier mass balance to the mountain range scale: the European Alps 1900–2100. The Cryosphere Discuss 6:1117–1156

IPCC (2019) Chapter 2: High Mountain Areas — Special Report on the Ocean and Cryosphere in a Changing Climate

Jibson RW, Harp EL, Schulz W, Keefer DK (2006) Large rock avalanches triggered by the M 7.9 Denali Fault, Alaska, earthquake of 3 November 2002. Engineering Geology 83:144–160. https://doi.org/10.1016/j.enggeo.2005.06.029

Knoflach B, Tussetschläger H, Sailer R, et al (2021) High mountain rockfall dynamics: rockfall activity and runout assessment under the aspect of a changing cryosphere. Geografiska Annaler: Series A, Physical Geography 0:1–20. https://doi.org/10.1080/04353676.2020.1864947

Krautblatter M, Funk D, Günzel FK (2013) Why permafrost rocks become unstable: a rock–ice-mechanical model in time and space. Earth Surface Processes and Landforms 38:876–887. https://doi.org/10.1002/esp.3374

Lan H, Zhang Y, Macciotta R, et al (2022) The role of discontinuities in the susceptibility, development, and runout of rock avalanches: a review. Landslides 19:1391–1404. https://doi.org/10.1007/s10346-022-01868-w

Legay A, Magnin F, Ravanel L (2021) Rock temperature prior to failure: analysis of 209 rockfall events in the Mont Blanc massif (Western European Alps). Permafrost and Periglacial Processes 32:520–536. https://doi.org/10.1002/ppp.2110

Li L, Lan H (2015) Probabilistic modeling of rockfall trajectories: a review. Bull Eng Geol Environ 74:1163–1176. https://doi.org/10.1007/s10064-015-0718-9

Lied K (1977) Rockfalls problems in Norway. ISMES 51–53

Loye A, Jaboyedoff M, Pedrazzini A (2009) Identification of potential rockfall source areas at a regional scale using a DEM-based geomorphometric analysis. Natural Hazards and Earth System Sciences 9:1643–1653. https://doi.org/10.5194/nhess-9-1643-2009

Magnin F, Josnin J-Y (2021) Water Flows in Rock Wall Permafrost: A Numerical Approach Coupling Hydrological and Thermal Processes. Journal of Geophysical Research: Earth Surface 126:e2021JF006394. https://doi.org/10.1029/2021JF006394

Magnin F, Brenning A, Bodin X, et al (2015a) Modélisation statistique de la distribution du permafrost de paroi : application au massif du Mont Blanc. Géomorphologie : relief, processus, environnement 21:145–162. https://doi.org/10.4000/geomorphologie.10965

Magnin F, Krautblatter M, Deline P, et al (2015b) Determination of warm, sensitive permafrost areas in near-vertical rockwalls and evaluation of distributed models by electrical resistivity tomography. Journal of Geophysical Research: Earth Surface 120:745–762. https://doi.org/10.1002/2014JF003351

Magnin F, Josnin J-Y, Ravanel L, et al (2017) Modelling rock wall permafrost degradation in the Mont Blanc massif from the LIA to the end of the 21st century. The Cryosphere 11:1813–1834. https://doi.org/10.5194/tc-11-1813-2017

Magnin F, Haeberli W, Linsbauer A, et al (2020) Estimating glacier-bed overdeepenings as possible sites of future lakes in the de-glaciating Mont Blanc massif (Western European Alps). Geomorphology 350:106913. https://doi.org/10.1016/j.geomorph.2019.106913

Mamot P, Weber S, Schröder T, Krautblatter M (2018) A temperature- and stress-controlled failure criterion for ice-filled permafrost rock joints. The Cryosphere 12:3333–3353. https://doi.org/10.5194/tc-12-3333-2018

Mamot P, Weber S, Eppinger S, Krautblatter M (2021) A temperature-dependent mechanical model to assess the stability of degrading permafrost rock slopes. Earth Surface Dynamics 9:1125–1151. https://doi.org/10.5194/esurf-9-1125-2021

Marcer M, Bodin X, Brenning A, et al (2017) Permafrost Favorability Index: Spatial Modeling in the French Alps Using a Rock Glacier Inventory. Front Earth Sci 5:. https://doi.org/10.3389/feart.2017.00105

McColl ST (2012) Paraglacial rock-slope stability. Geomorphology 153–154:1–16. https://doi.org/10.1016/j.geomorph.2012.02.015

McColl ST, Draebing D (2018) Rock Slope Instability in the Proglacial Zone: State of the Art. In: Heckmann T, Morche D (eds) Geomorphology of Proglacial Systems: Landform and Sediment Dynamics in Recently Deglaciated Alpine Landscapes. Springer International Publishing, Cham, pp 119–141

Menk J, Berger F, Moos C, Dorren L (2023) Towards an improved rapid assessment tool for rockfall protection forests using field-mapped deposited rocks. Geomorphology 422:108520. https://doi.org/10.1016/j.geomorph.2022.108520

Mergili M, Marchesini I, Alvioli M, et al (2014) A strategy for GIS-based 3-D slope stability modelling over large areas. Geoscientific Model Development 7:2969–2982. https://doi.org/10.5194/gmd-7-2969-2014

Mergili M, Fischer J-T, Krenn J, Pudasaini SP (2017) r.avaflow v1, an advanced open-source computational framework for the propagation and interaction of two-phase mass flows. Geoscientific Model Development 10:553–569. https://doi.org/10.5194/gmd-10-553-2017

Mergili M, Schwarz L, Kociu A (2019) Combining release and runout in statistical landslide susceptibility modeling. Landslides 16:2151–2165. https://doi.org/10.1007/s10346-019-01222-7

Michoud C, Derron M-H, Horton P, et al (2012) Rockfall hazard and risk assessments along roads at a regional scale: example in Swiss Alps. Natural Hazards and Earth System Sciences 12:615–629. https://doi.org/10.5194/nhess-12-615-2012

Mourey J, Lacroix P, Duvillard P-A, et al (2022) Multi-method monitoring of rockfall activity along the classic route up Mont Blanc (4809 m a.s.l.) to encourage adaptation by mountaineers. Natural Hazards and Earth System Sciences 22:445–460. https://doi.org/10.5194/nhess-22-445-2022

Noetzli J, Huggel C, Hoelzle M, Haeberli W (2006) GIS-based modelling of rock-ice avalanches from Alpine permafrost areas. Computational Geosciences 10:161–178. https://doi.org/10.1007/s10596-005-9017-z

Paranunzio R, Chiarle M, Laio F, et al (2019) Slope failures in high-mountain areas in the Alpine Region. Supplement to: Paranunzio, R et al. (2019): New insights in the relation between climate and slope failures at high-elevation sites. Theoretical and Applied Climatology, 137(3-4), 1765-1784, https://doi.org/10.1007/s00704-018-2673-4

Pecoraro G, Calvello M, Piciullo L (2019) Monitoring strategies for local landslide early warning systems. Landslides 16:213–231. https://doi.org/10.1007/s10346-018-1068-z

Penna IM, Magnin F, Nicolet P, et al (2023) Permafrost controls the displacement rates of large unstable rock-slopes in subarctic environments. Global and Planetary Change 220:104017. https://doi.org/10.1016/j.gloplacha.2022.104017

Ravanel L, Deline P (2011) Climate influence on rockfalls in high-Alpine steep rockwalls: The north side of the Aiguilles de Chamonix (Mont Blanc massif) since the end of the 'Little Ice Age.' The Holocene 21:357–365. https://doi.org/10.1177/0959683610374887

Ravanel L, Deline P (2013) A network of observers in the Mont Blanc massif to study rockfalls in high alpine rockwalls. Geografia Fisica e Dinamica Quaternaria 36: https://doi.org/10.4461/GFDQ.2013.36.12

Ravanel L, Allignol F, Deline P, et al (2010) Rock falls in the Mont Blanc Massif in 2007 and 2008. Landslides 7:493–501. https://doi.org/10.1007/s10346-010-0206-z

Ravanel L, Lambiel C, Reynard E, et al (2011) Les écroulements rocheux dans le massif du Mont Blanc pendant l'été caniculaire de 2003. Géovisions 36:225–241

Ravanel L, Deline P, Lambiel C, Vincent C (2013) Instability of a highly vulnerable high alpine rock ridge: the lower Arête des Cosmiques (Mont Blanc massif, France). Geografiska Annaler: Series A, Physical Geography 95:51–66. https://doi.org/10.1111/geoa.12000

Ravanel L, Magnin F, Deline P (2017) Impacts of the 2003 and 2015 summer heatwaves on permafrost-affected rock-walls in the Mont Blanc massif. Science of The Total Environment 609:132–143. https://doi.org/10.1016/j.scitotenv.2017.07.055

Scheidegger AE (1973) On the prediction of the reach and velocity of catastrophic landslides. Rock Mechanics 5:231–236. https://doi.org/10.1007/BF01301796

Shugar DH, Jacquemart M, Shean D, et al (2021) A massive rock and ice avalanche caused the 2021 disaster at Chamoli, Indian Himalaya. Science 373:300–306. https://doi.org/10.1126/science.abh4455

Sosio R, Crosta GB, Chen JH, Hungr O (2012) Modelling rock avalanche propagation onto glaciers. Quaternary Science Reviews 47:23–40

Stead D, Wolter A (2015) A critical review of rock slope failure mechanisms: The importance of structural geology. Journal of Structural Geology 74:1–23. https://doi.org/10.1016/j.jsg.2015.02.002

Temme AJAM (2015) Using climber's guidebooks to assess rock fall patterns over large spatial and decadal temporal scales: an example from the swiss alps: Geografiska Annaler: Series A, Physical Geography: Vol 97, No 4. Geografiska Annaler: Series A, Physical Geography 97:793–807. https://doi.org/DOI :10.1111/geoa.12116

Verfaillie D, Lafaysse M, Déqué M, et al (2018) Multi-component ensembles of future meteorological and natural snow conditions for 1500 m altitude in the Chartreuse mountain range, Northern French Alps. The Cryosphere 12:1249–1271. https://doi.org/10.5194/tc-12-1249-2018

Walter F, Amann F, Kos A, et al (2020) Direct observations of a three million cubic meter rock-slope collapse with almost immediate initiation of ensuing debris flows. Geomorphology 351:106933. https://doi.org/10.1016/j.geomorph.2019.106933

Wegmann M, Gudmundsson GH, Haeberli W (1998) Permafrost changes in rock walls and the retreat of alpine glaciers: a thermal modelling approach. Permafrost and Periglacial Processes 9:23–33. https://doi.org/10.1002/(SICI)1099-1530(199801/03)9:1<23::AID-PPP274>3.0.CO;2-Y

Zekollari H, Huss M, Farinotti D (2019) Modelling the future evolution of glaciers in the European Alps under the EURO-CORDEX RCM ensemble. The Cryosphere 13:1125–1146. https://doi.org/10.5194/tc-13-1125-2019

Zemp M, Haeberli W, Hoelzle M, Paul F (2006) Alpine glaciers to disappear within decades? Geophysical Research Letters 33:. https://doi.org/10.1029/2006GL026319

Zevenbergen LW, Thorne CR (1987) Quantitative analysis of land surface topography. Earth Surface Processes and Landforms 12:47–56. https://doi.org/10.1002/esp.3290120107

Zheng G, Mergili M, Emmer A, et al (2021) The 2020 glacial lake outburst flood at Jinwuco, Tibet: causes, impacts, and implications for hazard and risk assessment. The Cryosphere 15:3159–3180. https://doi.org/10.5194/tc-15-3159-2021